Quantum Theory for the Computer Age

Unit 5

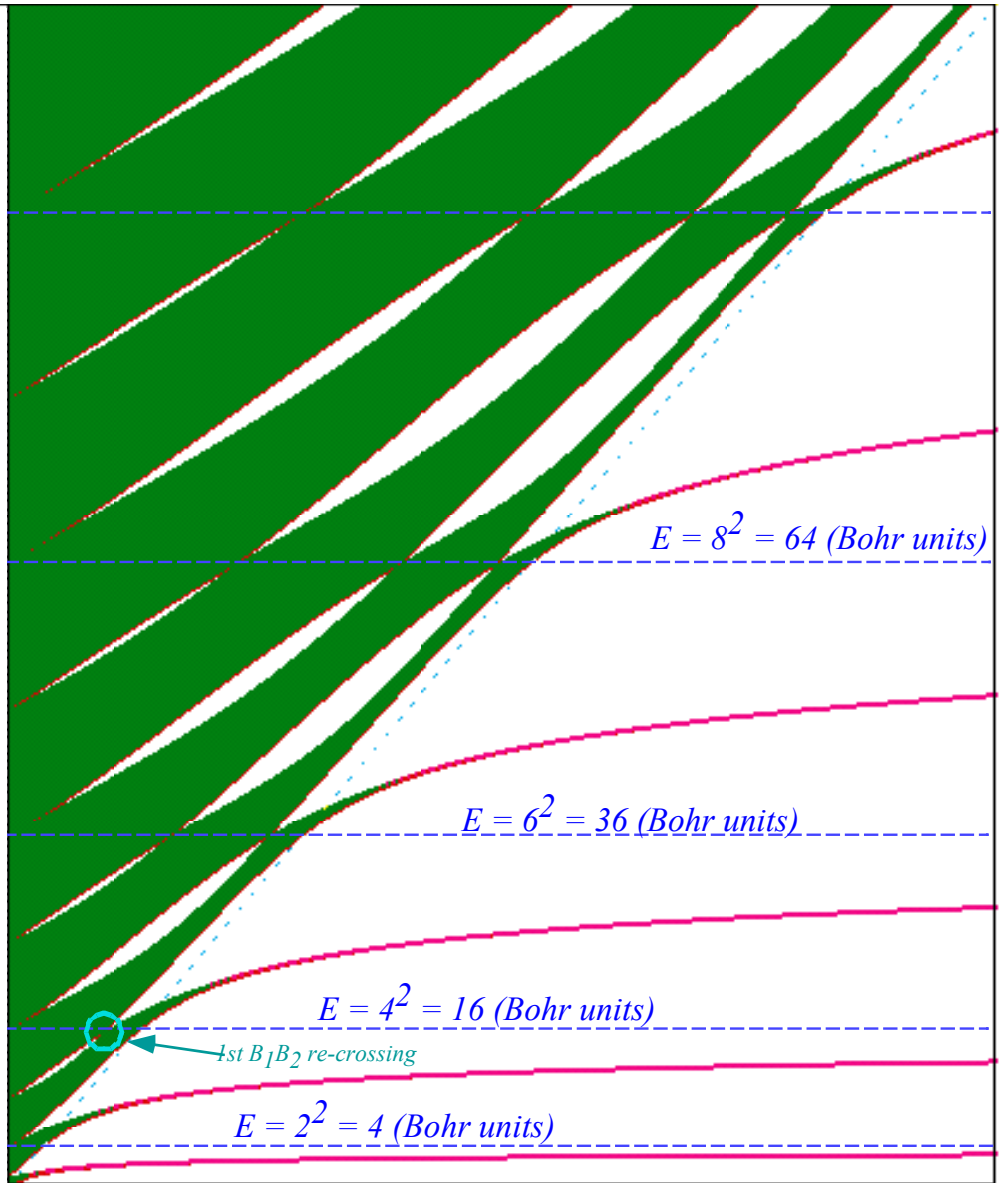

Multiple Barriers and Resonance Bands

Unit 5 Periodic Potentials

Unit 4 introduced the Schrodinger time equation with piecewise constant potential barriers and wells with their strong distinction between resonance in a continuum and discrete bound states. This Unit 5 introduces periodic potential barriers for which these distinctions begin to disappear. In the real world every state is a resonance; some are more so but nothing lives forever. Symmetry is a key property that encourages high quality resonance because it means having two or more parts that are similar or identical and this implies frequencies that are similar or identical, the *sin qua non* for resonance. Examples are given of potential well systems with symmetry equal to or greater than that of the C_n sytems of Unit 3 Chapter 9. Energy bands and states of periodic potentials are introduced using the ideas of resonant and nonresonant eigenchannels introduced in the preceding Chapter 13. Kronig –Penney solutions are related to resonance band structure in Chapter 14, to non-commutative symmetry group algebra in Chapter 15, and to different flavors of Fourier symmetry analysis in Chapter 16.

W. G. Harter

Department of Physics

University of Arkansas

Fayetteville

Hardware and Software by

HARTER-*Soft*

Elegant Educational Tools Since 2001

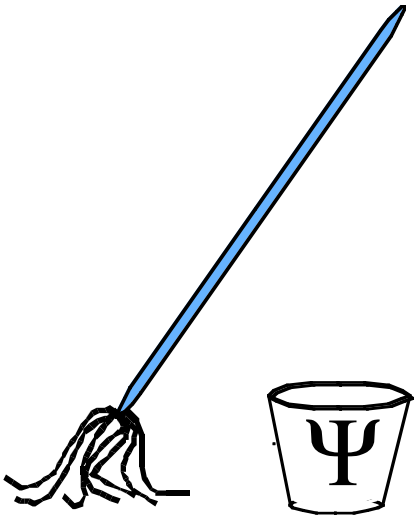

QM for AMOP

Chapter 14

Multiple Barriers and Resonance Bands

W. G. Harter

The preceding Chapter 13 dealt with simple potential well and barrier states in what amounted to minimum-security prisons. This Chapter 14 deals with more clever forms of wave incarceration involving repeated sets of barriers and quantum wells that resemble the discrete C_N-symmetric quantum dot structures of Chapters 8 and 9. While the latter had discrete spectra, the quantum wells described in this Chapter have a continuous spectrum, but it is peppered with resonance bands and wave states quite like the discrete C_N-bands. Now the distinction becomes blurred between the free and the imprisoned or continuous and discrete; they're two sides of the same coin!

Chapter 14. Multiple Barriers and Resonance Bands

14.1 Waves and Potential Barriers: Crossing Matrices

A revealing approach to the band theory of solids involves stringing together multiple copies of barriers and wells in various symmetric arrays or sequences. In Sec. 13.1 (b) we noted that the crossing matrix for a sequence of potential structures is the matrix product of the *C*-matrices of the component sub-structures. If each sub-structure is the same except for its location, then the component *C*-matrices all have the same form and nearly the same numerical values differing only in phase factors here and there.

(a) Well-well

Consider stringing two identical wells together as in Fig. 14.1.1.

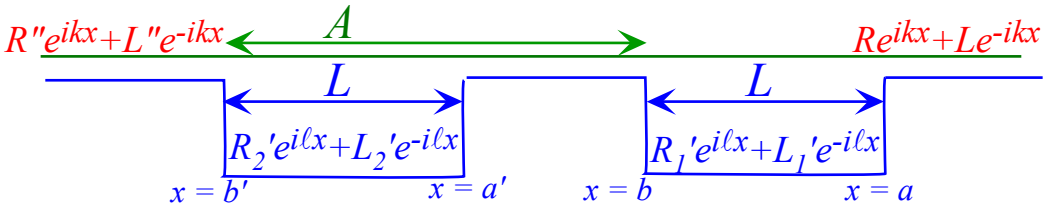

Fig. 14.1.1 C_2-symmetric double square well .

Using the preceding *C*-matrix (13.3.33) in a product yields the desired well-well or (well)^2 *C*-matrix.

$$\begin{pmatrix} R'' \\ L'' \end{pmatrix} = C' \cdot C \begin{pmatrix} R \\ L \end{pmatrix} = \begin{pmatrix} e^{ikL}\chi^* & -ie^{-ik(a'+b')}\xi \\ ie^{ik(a'+b')}\xi & e^{-ikL}\chi \end{pmatrix} \cdot \begin{pmatrix} e^{ikL}\chi^* & -ie^{-ik(a+b)}\xi \\ ie^{ik(a+b)}\xi & e^{-ikL}\chi \end{pmatrix} \begin{pmatrix} R \\ L \end{pmatrix}$$
$$= \begin{pmatrix} e^{i2kL}\chi^2 + e^{-i2kA}\xi^2 & -i\xi\left(e^{-i2kb}\chi^* + e^{-i2ka'}\chi\right) \\ i\xi\left(e^{i2kb}\chi + e^{i2ka'}\chi^*\right) & e^{-i2kL}\chi^2 + e^{i2kA}\xi^2 \end{pmatrix} \begin{pmatrix} R \\ L \end{pmatrix} \qquad (14.1.1a)$$

where the following matrix components are defined:

$$\chi = \cos \ell L + i \cosh 2\alpha \sin \ell L \quad \text{and:} \quad \xi = \sinh 2\alpha \sin \ell L \qquad (14.1.1b)$$

The well-length *L* and distance or *lattice constant A* between wells are, respectively, the following.

$$L = a - b = a' - b' \quad \text{and,} \quad A = a - a' = b - b' \qquad (14.1.1c)$$

The kinetic factors are a repeat of those in (13.3.33c).

$$\cosh 2\alpha = \frac{1}{2}\left(\frac{\ell}{k} + \frac{k}{\ell}\right) = \frac{\ell^2 + k^2}{2k\ell}, \qquad \sinh 2\alpha = \frac{1}{2}\left(\frac{\ell}{k} - \frac{k}{\ell}\right) = \frac{\ell^2 - k^2}{2k\ell}, \qquad (14.1.1d)$$

As shown just before equation (13.1.25), a resonance has zero reflection, that is, $L'' = 0$ or

$$0 = L'' = C_{21}R = i\xi\left(e^{i2kb}\chi + e^{i2ka'}\chi^*\right)R \, . \qquad (14.1.2)$$

This also implies perfect transmission *(*$|T|=1$*)* with the following inverse transmission ratio.

$$1/\sqrt{|T|} = |R''|/|R| = 1 = |C_{11}| = \left|e^{i2kL}\chi^2 + e^{-i2kA}\xi^2\right| . \qquad (14.1.3)$$

For energy below barrier *V*, this ratio, with $ik=-\kappa$, goes to zero for bound states. (Recall Fig. 13.2.2.)

$$|R''|/|R| = |C_{11}| = \left|e^{-2\kappa L}\chi^2 + e^{2\kappa A}\xi^2\right| \to 0 \qquad (14.1.4)$$

For the double well, resonant and bound states come in nearly degenerate pairs. In Fig. 14.1.2 a and b are two orthogonal bound state waves for a potential $V=-25$ of width $L=1.5$ and separation $A=2.0$. The ground state (a) has energy $E(0^+) = -23.468$ and while the first excited state has energy $E(0^-) = -23.437$ is barely 0.03 above the ground state. The probability envelopes for the two states are practically indistinguishable except at the mid-point between the two wells where the excited state has a node but the ground state does not. This pair is analogous to the NH_3 inversion doublet discussed in Chapter 10.

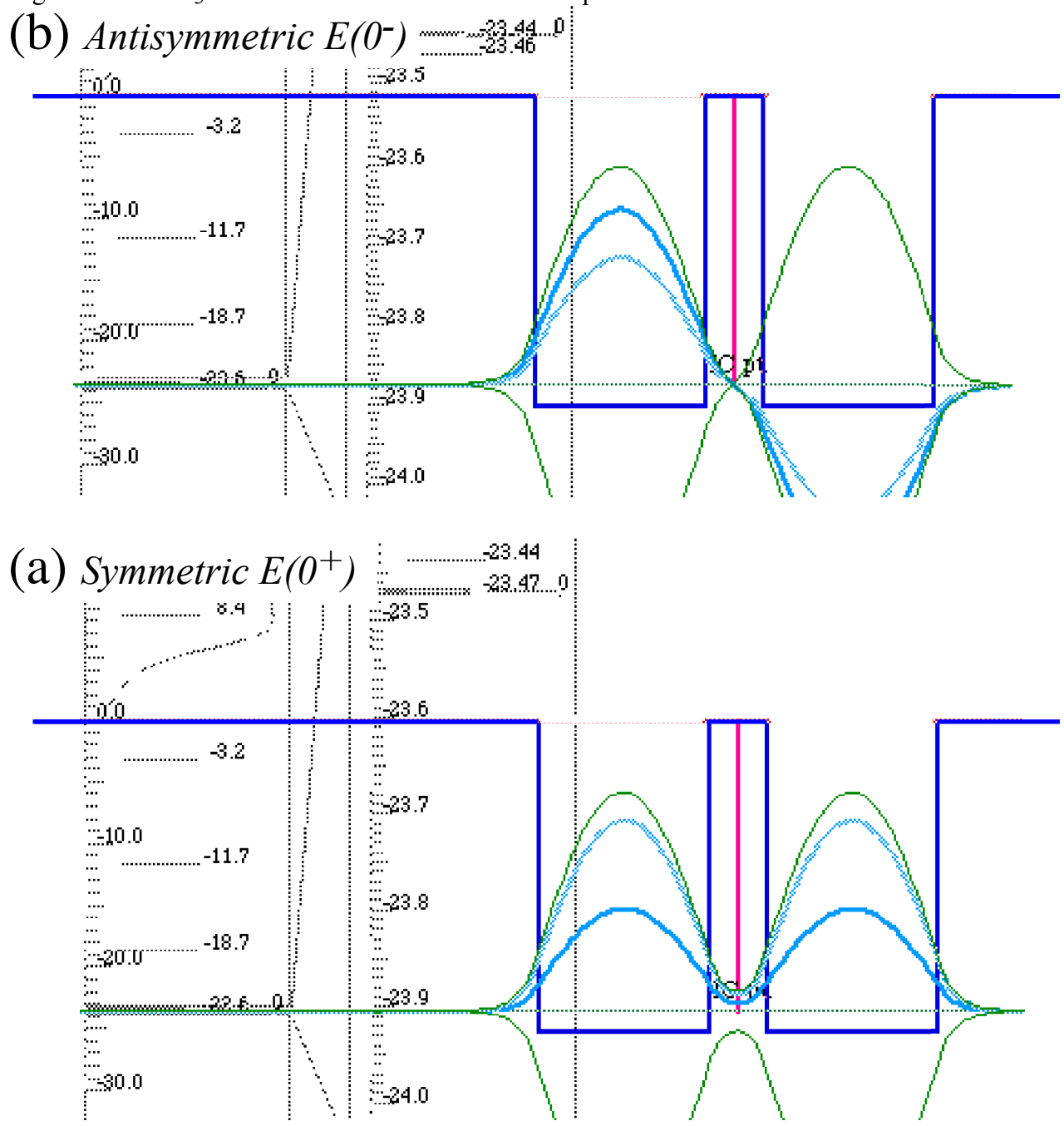

Fig. 14.1.2 Lowest inversion-doublet pair in double well . (a) Symmetric, (b) Anti-symmetric

Energy eigenlevels $E(1^+) = -18.96$ and $E(1^-) = -18.81$ are paired, too, into an antisymmetric and symmetric set of waves shown in Fig. 14.1.3 a and b. However, now energy difference $\Delta E=0.15$ is not quite so small.

(b) *Antisymmetric E(1⁻)*

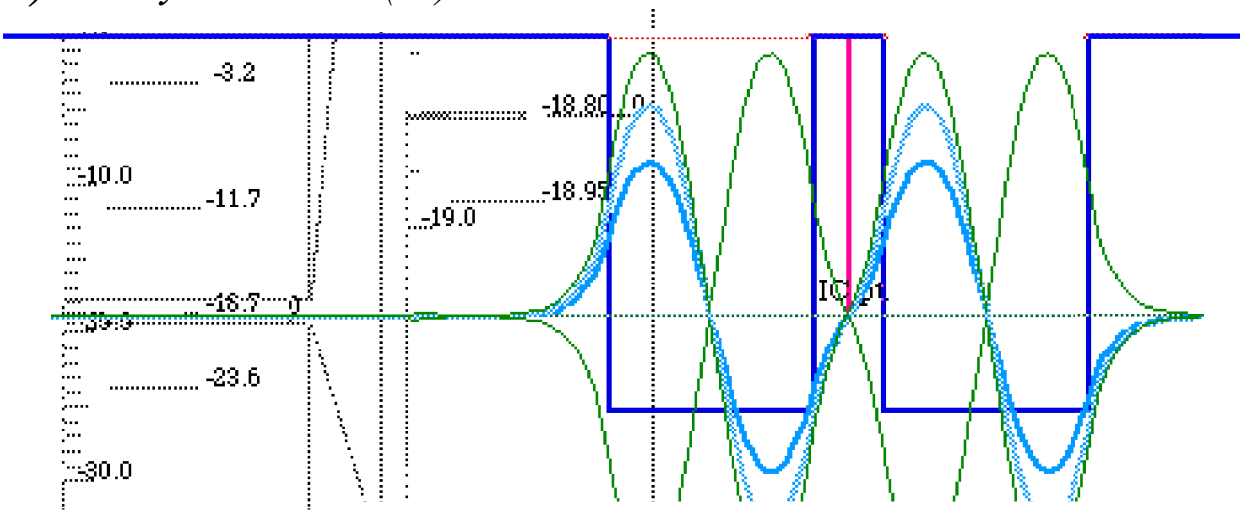

(a) *Symmetric E(1⁺)*

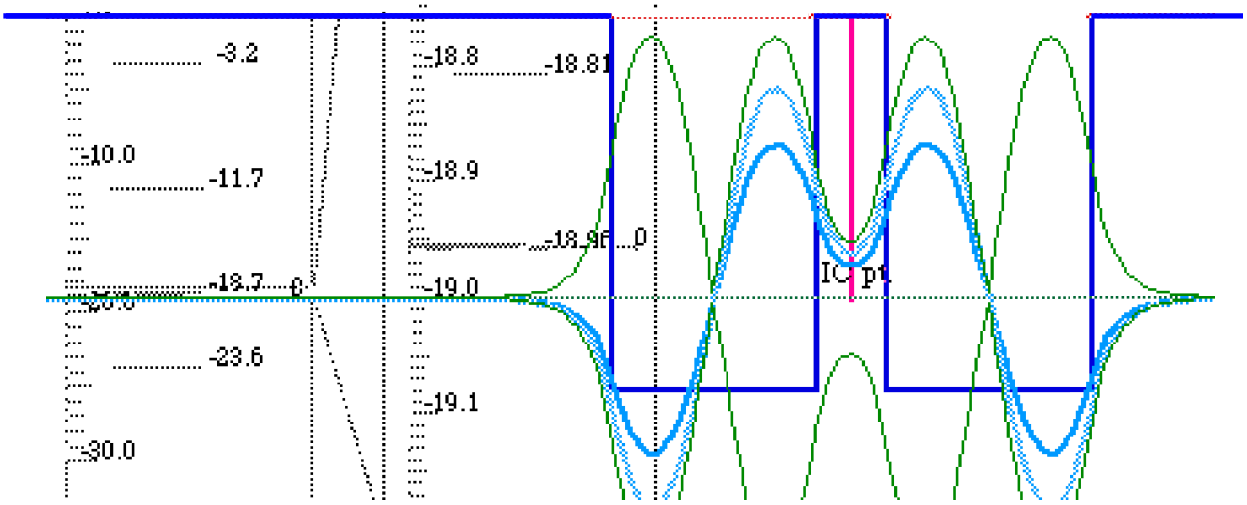

Fig. 14.1.3 Next lowest inversion-doublet pair in double well . (a) Symmetric, (b) Anti-symmetric

Each eigenlevel of the single well namely, *E(0)= -23.453*, *E(1)= -18.88* , and so forth, is found to lie nearly midway between an inversion doublet pair of the double-well potential. In other words, each pair is described by the familiar 2-state bilaterally symmetric *B*-type Hamiltonian matrix from (10.2.4c).

$$\begin{pmatrix} \langle 1|\mathbf{H}|1\rangle & \langle 1|\mathbf{H}|2\rangle \\ \langle 2|\mathbf{H}|1\rangle & \langle 2|\mathbf{H}|2\rangle \end{pmatrix} = \begin{pmatrix} A & B \\ B & A \end{pmatrix} = \begin{pmatrix} H & -S \\ -S & H \end{pmatrix} \qquad (14.1.5)$$

Here $\Delta E=2S$ is the splitting between each pair of double well states having energy $E^+=H-S$ or $E^-=H+S$. This notation was adapted in the NH_3 discussion beginning with (10.3.3).

The beat dynamics of the waves in Figs. 14.1.2-3 are the same as that which was discussed in Chapter 10.2b. A mixture of an n^+ and n^- state (particularly a 50-50 mixture) results in a beat oscillation back and forth at the difference or tunneling frequency $\Delta E/\hbar = 2S/\hbar$. The only difference is that these frequencies can be exponentially small for pairs that lie deep down in their respective wells. Then tunneling looks more like a diffusive "oozing" process than a resonant process that it must be.

Resonance states also come in pairs. The transmission spectrum for a pair of nearest grazing resonances in Fig. 14.1.4 shows a barely resolved doublet corresponding to resonances $E(4^+) = +8.4$ and $E(4^-) = +10.0$. The waves shown belong to carefully prepared *S*-matrix eigenchannel states using the center of symmetry as the origin. Note how the symmetric wave piles up more charge on the central barrier than the antisymmetric wave which has a node at origin. For a more nearly grazing resonance this charge localization effect is even more pronounced, particularly with a narrow central barrier like this potential.

At higher energy or for thicker separation barriers, the barrier-top resonances such as pictured in Fig. 13.1.6, will contribute to transmission variation along with the intra-well resonances shown here in Fig. 14.1.4. Later on in Sec. 14.2 (c-3), we shall encounter situations where the two occur together. As pointed out in previous discussions (For example, recall Fig. 13.1.7.), much of this sharp resonance phenomena owe their existence to sharp-walled potentials with flat tops!

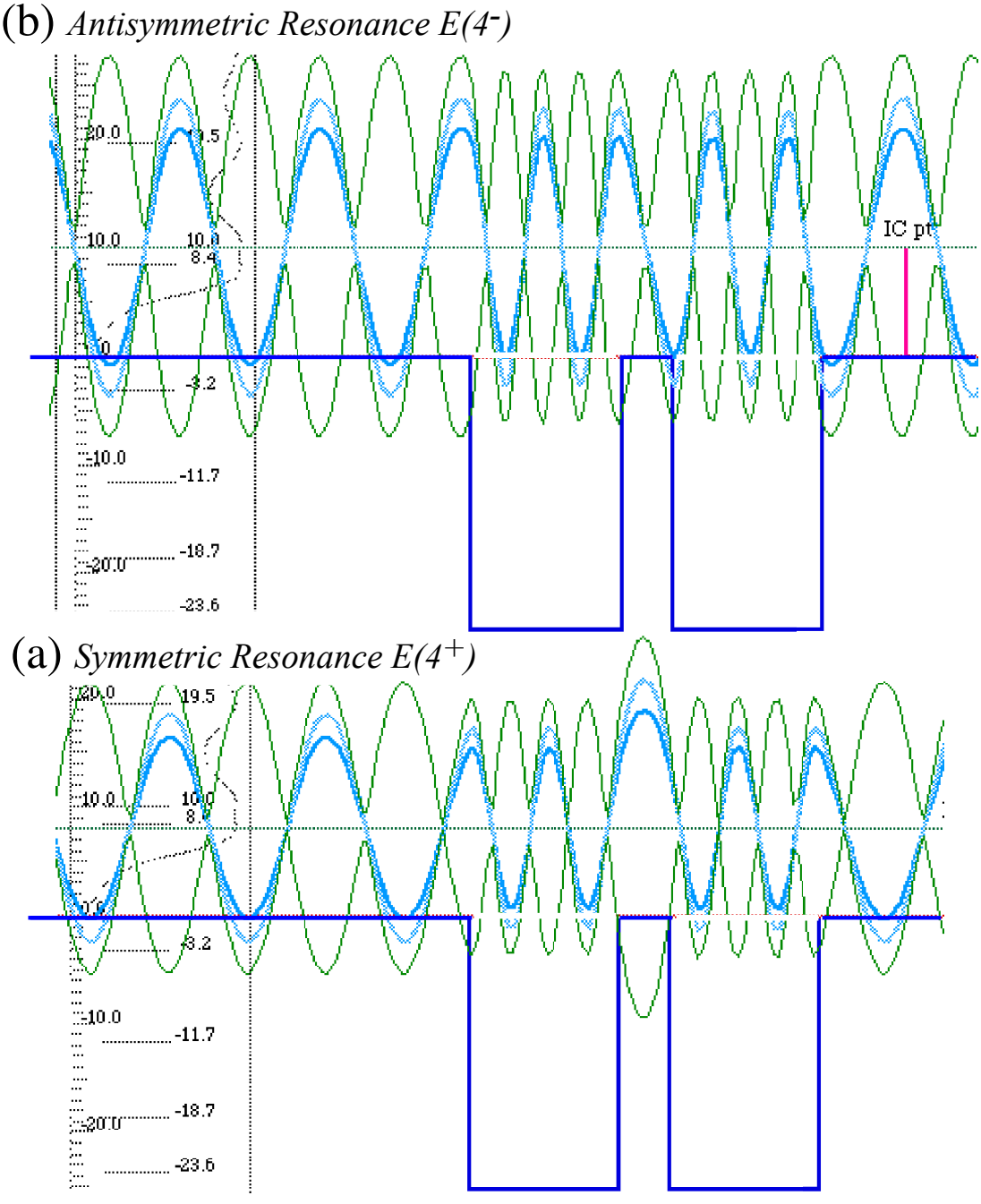

Fig. 14.1.4 Resonance-doublet pair above double well . (a) Symmetric, (b) Anti-symmetric

(b) Hump-hump

The same equations (14.1.1) with minor changes apply to a pair of humps shown in Fig. 14.1.5.

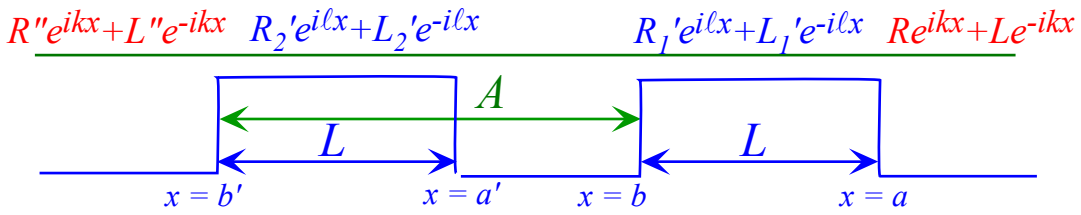

Fig. 14.1.5 C_2-symmetric double barrier .

No modification of (14.1.1) is needed as long as the energy E is above the barrier top V.

$$\begin{pmatrix} R'' \\ L'' \end{pmatrix} = \begin{pmatrix} e^{i2kL}\chi^2 + e^{-i2kA}\xi^2 & -i\xi\left(e^{-i2kb}\chi^* + e^{-i2ka'}\chi\right) \\ i\xi\left(e^{i2kb}\chi + e^{i2ka'}\chi^*\right) & e^{-i2kL}\chi^2 + e^{i2kA}\xi^2 \end{pmatrix} \begin{pmatrix} R \\ L \end{pmatrix} \qquad (14.1.6)$$

However, if $E<V$, the wavevector ℓ is replaced by iκ, i times an evanescent parameter, and the following matrix components are redefined accordingly from those of (14.1.1b),

$$\chi = \cosh \kappa L - i \sinh 2\beta \ \sinh \kappa L, \ \text{and:} \ \xi = \cosh 2\beta \ \sinh \kappa L, \qquad (14.1.7)$$

using barrier parameters in (13.3.34).

$$\cosh 2\beta = \frac{1}{2}\left(\frac{\kappa}{k} + \frac{k}{\kappa}\right) = \frac{\kappa^2 + k^2}{2k\kappa}, \quad \sinh 2\beta = \frac{1}{2}\left(\frac{\kappa}{k} - \frac{k}{\kappa}\right) = \frac{\kappa^2 - k^2}{2k\kappa} \qquad (14.1.8)$$

The main difference between the analysis of two wells and two humps is that the latter has no bound states; only resonances. However, the resonances are true *trapping resonances* in the sense that enormous amplification is easy to achieve, so they should be distinguished from the less spectacular Ramsauer-Townsend non-trapping resonances described so far.

For example, let us use the same depth $V=25$ and the same dimension $b\text{-}a' = 1.5$ for the interior well of Fig. 14.1.5 as was used for the width $L=1.5$ in the preceding example involving Fig. 14.1.1. The result is an enormous resonance shown in Fig. 14.1.6 when the energy is tuned to the lowest peak at $E = 1.546$. (Note that the top-relative energy is $-25+1.546 = -23.454$; very close to the lowest E value of the single-well bound state or the H-value of the double well in the preceding section.)

The resonance amplitude in the well is amplified by approximately the sum of the magnitudes of the C_{11} or C_{12} components of barrier matrix (13.3.34a) each of which contributes about *32*.

$$C_{12} = -i \cosh 2\beta \sinh \kappa L = -31.8i \quad (\text{for } k = 6.8, \kappa = 1.76, L = 0.5)$$

So this resonance ends up with about *64* times the amplitude of the incoming wave or $64^2=4096$ times the intensity! By making the barriers thicker or higher we increase this amplification exponentially. (Recall single barrier tunneling problem 2.3.)

With amplitudes amplified so much you can expect that the sensitivity of the eigenchannel combinations will be extreme, too. Such strongly resonant systems are very sensitive to input amplitudes and phases as well as to changes in energy.

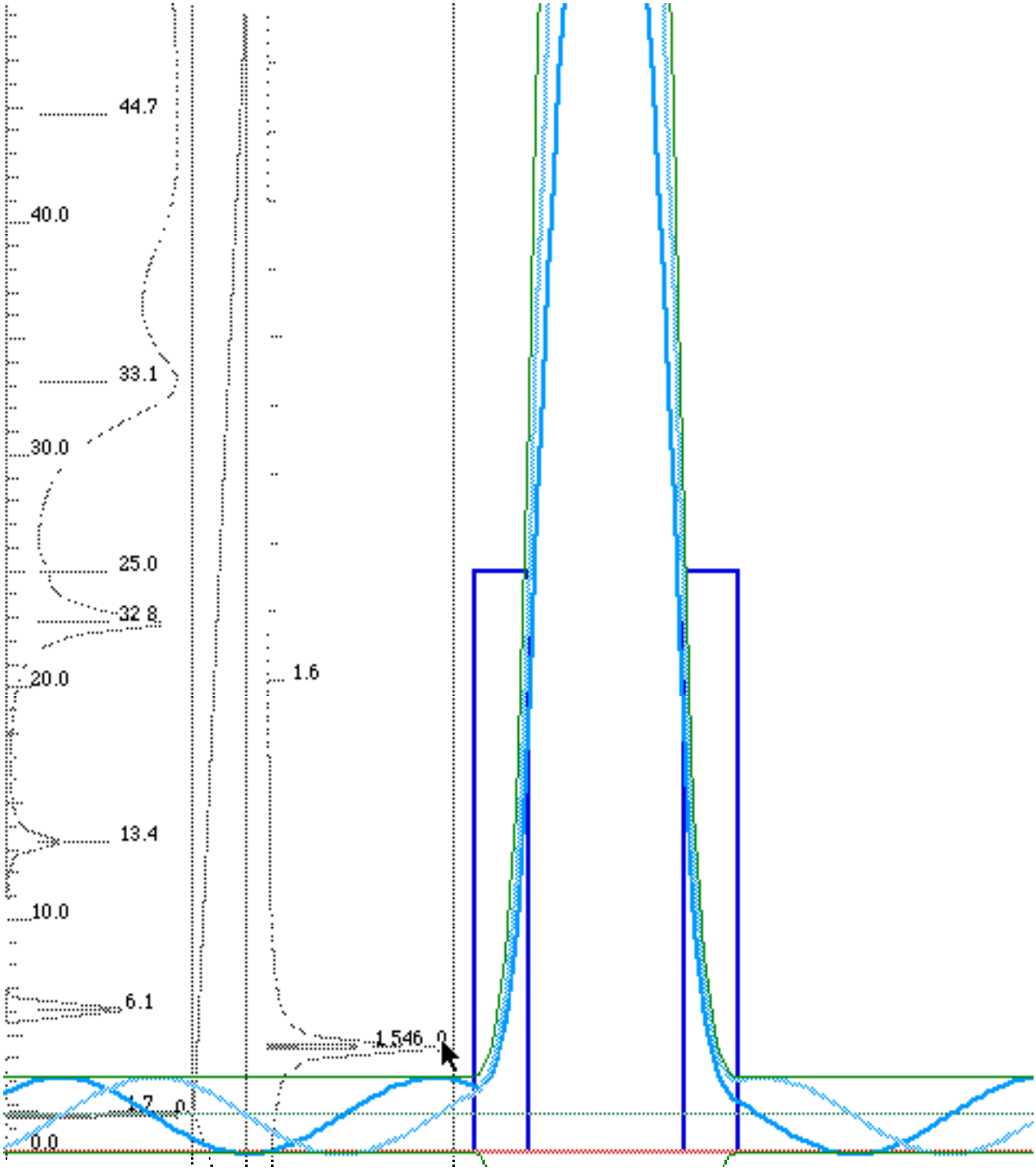

Fig. 14.1.6 Lowest (E= 1.546) resonance in L=0.5 well between two width=0.5 barriers(V=25) .

The next lowest resonance at (*E= 6.117 or -25+6.117 =-18.883*) is shown in Fig. 14.1.7. It is an antisymmetric wave with one node in the well. It has less amplification than the monster in Fig. 14.1.6, but still amounts to a gain of about 100 in intensity.

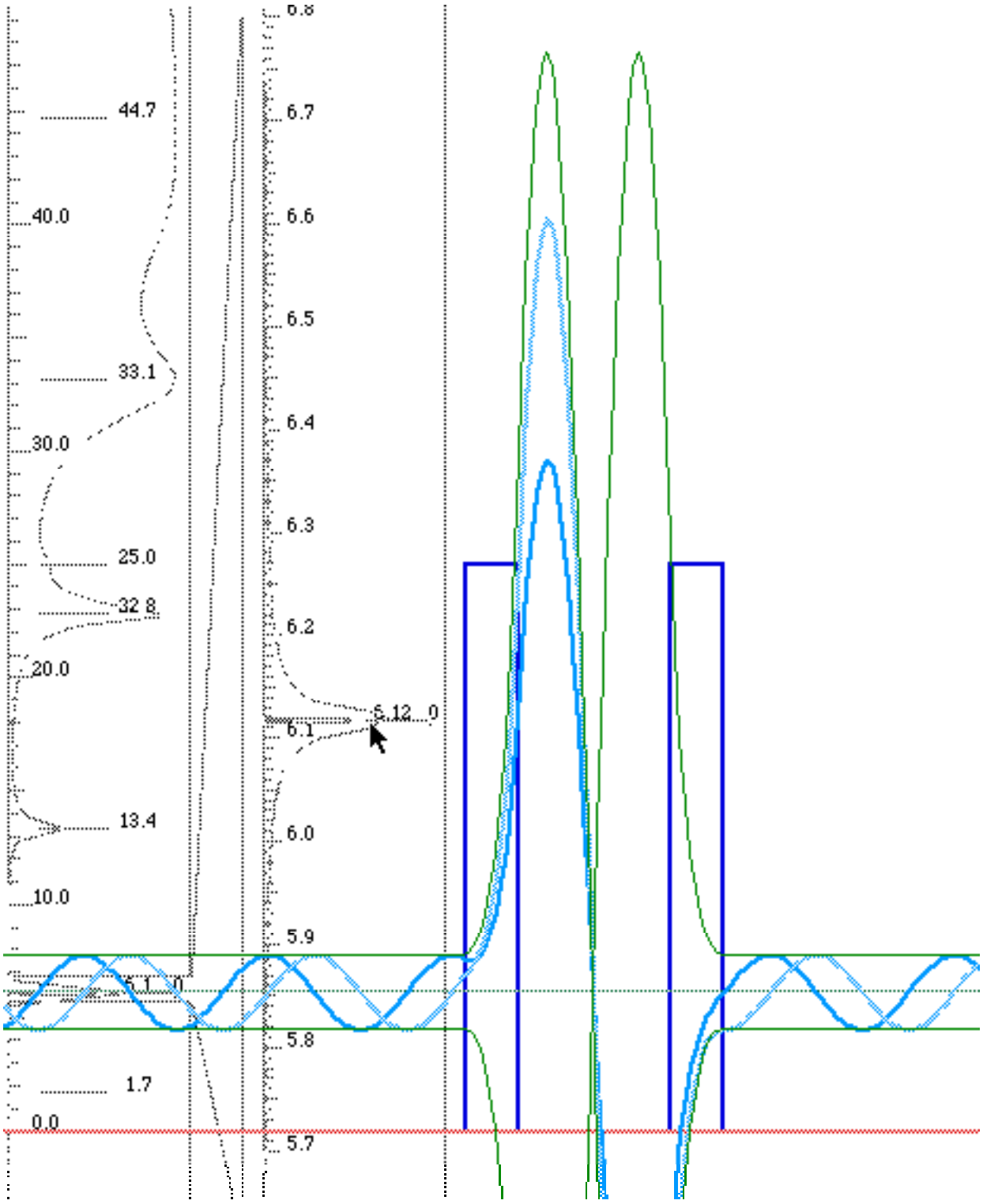

Fig. 14.1.7 Second (E= 6.117) resonance in L=0.5 well between two width=0.5 barriers(V=25) .

(1) C-and-S-Matrix Analytic properties: Resonance Widths and Lifetimes

Resonances in the preceding Fig. 14.1.6-7 can be made to exponentially approach bound states by raising or thickening the barriers. Even the flimsy walls used in the examples are sufficient to give resonance energies that approximate with 4-figure accuracy the bound-state energy eigenvalues for the same *(height = V =25, width = W =1.5)* well with infinitely thick walls. (See also Section 14.1(f).)

We have previously (in (14.1.4) and (13.2.2)) associated bound states with zeros of the ratio *R″/R* or, equivalently, poles of the ratio *R/R″*. Bound states require the amplitude *R″* of the right moving wave $e^{i(kx - \omega t)}$ to vanish when the wavevector factor *ik* becomes a real evanescent parameter -κ to avoid an exponential blow-up of $e^{-\kappa x}$ on the left side as *x* approaches -∞. On the other side, amplitude *R* of the same wave can be non-zero since $e^{-\kappa x}$ vanishes automatically on the right hand side as *x* approaches +∞.

So zeros of *C*-matrix component C_{11}, or equivalently, poles of *S*-matrix component $S_{12} = 1/C_{11}$, correspond to bound states if the wavevector becomes imaginary. Now we try a very strange but famous trick. We suppose that resonances for *real k* correspond to zeros of C_{11}, or equivalently, poles of S_{12} somewhere out in the *complex energy plane* but near the real *E*-axis.

The reasoning behind what seems, at first, to be crazy, is based on Fourier analysis. So far we haven't mixed states belonging to resonances and most of the pictures have been of states with a single energy carefully placed smack on top of a resonance peak. But, suppose for a minute that the peak is only the beginning of a huge (infinite) *S*-pole-mountain just below the real *E*-axis. More to the point, suppose C_{11} has a zero at complex energy $\hbar\,\Omega_n$ or complex frequency value $\Omega_n = \omega_n - i\,\Gamma_n$ just below the real resonance frequency ω_n. In other words, let the first Taylor-Laurent series expansion term of C_{11} be, for some coefficient c_n, as follows

$$C_{11}(\omega) = (\omega - \Omega_n)/c_n = (\omega - \omega_n + i\,\Gamma_n)/c_n \qquad (14.1.9)$$

in the neighborhood of Ω_n . Then the transmitted output amplitude *R* of the barrier system has the form

$$R_{k(\omega)} = \frac{1}{C_{11}(\omega)} R''_{k(\omega)} = \frac{c_n}{\omega - \Omega_n} R''_{k(\omega)} = \frac{c_n}{\omega - \omega_n + i\Gamma_n} R''_{k(\omega)} \qquad (14.1.10)$$

where we approximate coefficient c_n to be a constant in the neighborhood of the *n*-th resonance root Ω_n.

Suppose now that a continuous combination of near-resonant wave states are mixed together to make a non-stationary state whose wavefunction is approximately given by a frequency integral.

$$\Psi(x,t) = \int d\omega\; R_{k(\omega)} e^{i(kx - \omega t)} = \int d\omega\; \frac{c_n e^{i(kx - \omega t)}}{\omega - \omega_n + i\Gamma_n} R''_{k(\omega)}$$
$$\cong R''_{k(\omega_n)} c_n e^{ik(\omega_n)x} \int d\omega\; \frac{e^{-i\omega t}}{\omega - \omega_n + i\Gamma_n} \qquad (14.1.11)$$

Here we make approximations that you will see often in resonance theory. First, we suppose that the frequency distribution of the input amplitude $R''_{k(\omega)}$ is constant in the neighborhood of the resonance so it can go outside the integral. That is a good approximation since it could, in fact, be arranged. Next we move c_n outside, too, since it was previously assumed constant. This approximation depends on the approximate form of the *C*-matrix being what we said it was. (Not always so!) Finally, the wavevector $k(\omega)$ is assumed frozen at the resonance value $k(\omega_n)$. This is the most questionable of our approximations, and it will prevent us from seeing the group wave

interference outside of the barrier. However, since we are here interested only in rough overall time behavior this will be OK for now. Besides, it's the only way we can get a really simple analytic integral.

The integral itself is now approximated by appealing to *Cauchy's integral theorem* of complex *f(z)*.

$$\oint_C dz \frac{f(z)}{z-a} = \begin{cases} 0 & \text{if } a \text{ outside of contour } C, \\ 2\pi i\, f(a) & \text{if } a \text{ inside of contour } C. \end{cases} \qquad (14.1.12)$$

This is sometimes called *the residue theorem* and gives the value of an integral around a complex counter-clockwise contour *C* of a function *f(z)* (that has no poles inside *C*) divided by *(z-a)*. The value is *2πif(a)* or else zero depending on whether *a* is enclosed by contour *C* or not, respectively.

The integral (14.1.11) is a real integral but it can be made into a contour integral just like (14.1.12) by attaching a non-contributing "return loop" path that goes in ω-regions where the integrand, particularly the numerator $e^{-i\omega t}$, is practically zero. Such contours are sketched in Fig. 14.1.8. The upper contour is used for past time *(t<0)* because then ω=*i(large)* gives $e^{-i\omega t} = e^{(large)t}$ which is negligibly small for negative *t*. But, for the future times *(t >0)* we have to take the lower contour along which ω = *-i(large)* so, once again, the phasor values $e^{-i\omega t} = e^{-(large)t}$ are negligible for positive *t*. Either contour has to be big enough or far enough away from the pole to make $e^{-i\omega t}/(\omega - \Omega_n)$ have negligible magnitude on its return loop.

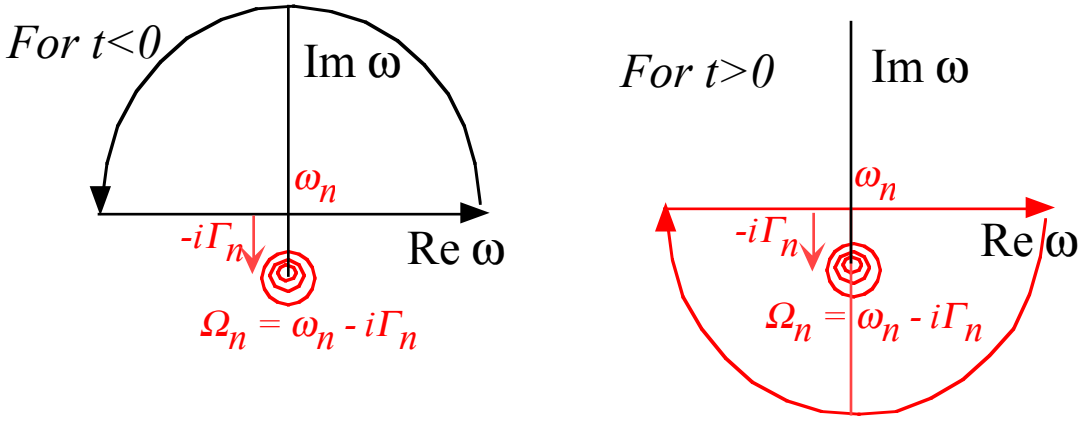

Fig. 14.1.8 Possible contours for resonance wave calculation.

The result of combining (14.1.11) and (14.1.12) is the following decaying ($e^{-\Gamma t}\, e^{-i\omega t}$)oscillation for *t > 0*.

$$\Psi(t) \cong \int d\omega\, \frac{e^{-i\omega t}}{\omega - \omega_n + i\Gamma_n} = \begin{cases} 0 & \text{for: } t<0 \\ -2\pi i\, e^{-i(\omega_n - i\Gamma_n)t} & \text{for: } t>0 \end{cases} \qquad (14.1.13)$$

The *resonance decay rate* Γ_n is just the distance the root of C_{11} or pole of S_{12} lies below the real-ω axis. The minus sign (on *-2πi*) is needed since the (*t>0*) contour goes clockwise or negatively.

It should be pointed out that roots of rational functions come in conjugate pairs. So the upper contour will also enclose a conjugate pole of the *S*-matrix component and the integral for past time will not be zero for the rational function as it is for our simple model approximation in (14.1.10).

How do we find the actual root displacement Γ_n or, for that matter, the real value ω_n of resonance frequency? Finding complex roots of functions like (14.1.7) is not trivial. An easy solution is to simply plot the

magnitude $|S_{12}(\omega)| = |1/C_{11}(\omega)|$ for real ω in the vicinity of each resonance and see how closely it fits the *model Lorentz resonance function* arising from the assumed form (14.1.10).

$$\left|\frac{1}{C_{11}(\omega)}\right|^2 = \left|\frac{c_n}{\omega-\omega_n+i\Gamma_n}\right|^2 = \frac{|c_n|^2}{(\omega-\omega_n)^2+\Gamma_n^2} \qquad (14.1.10)$$

If the fit is close, then accurate values for *resonance frequency* ω_n , *resonance decay rate* Γ_n, as well as *resonance peak strength* $|c_n/\Gamma_n|^2$ may be obtained fairly quickly. There is a little trick to this that comes from noting that the Lorenztian has half its peak value when $\omega-\omega_n = \pm\Gamma_n$. In other words, the decay rate Γ_n is the *Lorenztian Half-Width at Half-Maximum (HWHM)*.

Fig. 14.1.9(a) below shows a pretty close fit of a Lorentzian to a numerical plot (b) of the *13.45* resonance which is just above the *6.12* resonance in Fig. 14.1.7. This is a "textbook" resonance except for a slight "background" which "lifts" the numerical resonance peak and is due to the potential having thin walls and being slightly "transparent" at all frequencies.

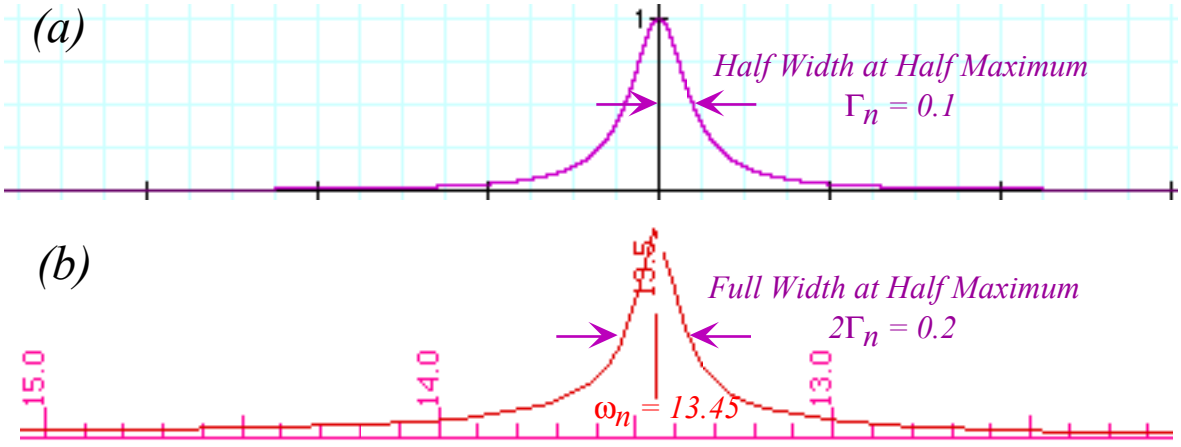

Fig. 14.1.9 Will the true Lorenztian please stand up!

We mentioned previously, that e^{-3} is nearly 5% so the *resonance 95% lifetime is* $3/\Gamma_n$. That's the time it would take for a "monster" like Fig. 14.1.6 to drain 95% of its amplitude if it was uniformly excited over its spectral band. Half that time, or $3/2\Gamma_n$ is what would be needed to drain 95% of its intensity or probability. The *probability decay rate* $2\Gamma_n$ is the *Lorenztian Full-Width at Half-Maximum (FWHM)*.

If the Lorentzian fit is not very close, then that says that this simple theory is wrong and some hidden mechanisms are present that need further study. The sub-grazing *22.8* resonance just below the *V=25* barrier top is an example. It appears to be "tipped" like a "hill-billy" living on mountain slope. The slope represents the growing transparency as energy approaches the barrier top. Shortly, we will see other examples of failure for simple Lorenztian fits such as happens with “clumps” of resonances. The first example in the following section deals with a pair of neighboring resonances.

(d) Hump-hump-hump

Let a third thin *(L=0.5)* wall be placed so that two wider *(W=1.5)* wells lie between three walls of height *(V=25)* as shown in Fig. 14.1.10 below.

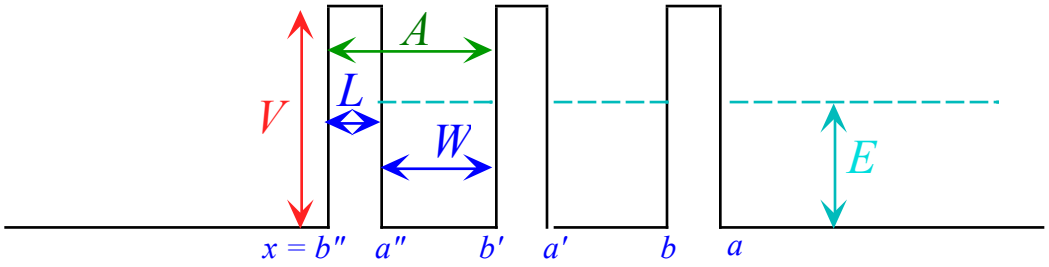

Fig. 14.1.10 Triple-barrier double-well potential

Each of the three barriers each has a *C*-matrix which enters a product to make the overall *C*-matrix.

$$C^{3-barrier} = C'' \cdot C' \cdot C$$
$$= \begin{pmatrix} e^{ikL}\chi^* & -ie^{-ik(a''+b'')}\xi \\ ie^{ik(a''+b'')}\xi & e^{-ikL}\chi \end{pmatrix} \cdot \begin{pmatrix} e^{ikL}\chi^* & -ie^{-ik(a'+b')}\xi \\ ie^{ik(a'+b')}\xi & e^{-ikL}\chi \end{pmatrix} \cdot \begin{pmatrix} e^{ikL}\chi^* & -ie^{-ik(a+b)}\xi \\ ie^{ik(a+b)}\xi & e^{-ikL}\chi \end{pmatrix} \quad (14.1.11a)$$

Except for the phases $k(a''+b'') = 2k\bar{x}''$, $k(a'+b') = 2k\bar{x}'$, and $k(a+b) = 2k\bar{x}$ at barrier centers, the parameters in the three matrices are identical. For energy below barrier top ($E<V$) the parameters are

$$\chi = \cosh \kappa L - i \sinh 2\beta \sinh \kappa L, \text{ and: } \xi = \cosh 2\beta \sinh \kappa L, \quad (14.1.11b)$$

using barrier coefficients from (14.1.7).

$$\cosh 2\beta = \frac{1}{2}\left(\frac{\kappa}{k} + \frac{k}{\kappa}\right) = \frac{\kappa^2 + k^2}{2k\kappa}, \qquad \sinh 2\beta = \frac{1}{2}\left(\frac{\kappa}{k} - \frac{k}{\kappa}\right) = \frac{\kappa^2 - k^2}{2k\kappa} \quad (14.1.11c)$$

Well wavevector k and barrier evanescence κ are given using rationalized (theorist units) energy ε and potential υ.

$$k = \sqrt{\frac{2mE}{\hbar^2}} = \sqrt{2\varepsilon}, \qquad \kappa = \sqrt{\frac{2m(V-E)}{\hbar^2}} = \sqrt{2(\upsilon - \varepsilon)}. \quad (14.1.11c)$$

The resonance transmission spectrum for the triple-barrier double-well is composed of pairs of peaks with each peak resembling a Lorentzian. The first three of these are plotted using scales of decreasing (with energy) magnification in Fig. 14.1.11. It is evident that a simple phenomenological modeling of each resonance cannot be done with a single Lorentzian but requires at least a *double Lorentzian*, something like that of a coupled damped two-dimensional pendulum system.

$$S_{12}(\omega) = \frac{1}{C_{11}(\omega)} = \frac{c(n^+)}{\omega - \omega(n^+) + i\Gamma(n^+)} + \frac{c(n^-)}{\omega - \omega(n^-) + i\Gamma(n^-)} \quad (14.1.12)$$

This model would require six parameters $c(n^{\pm})$, $\omega(n^{\pm})$, and $\Gamma(n^{\pm})$ for each resonance $n=0, 1, 2,...$, and that's too many. (It would be more like quantum chemistry than physics!)

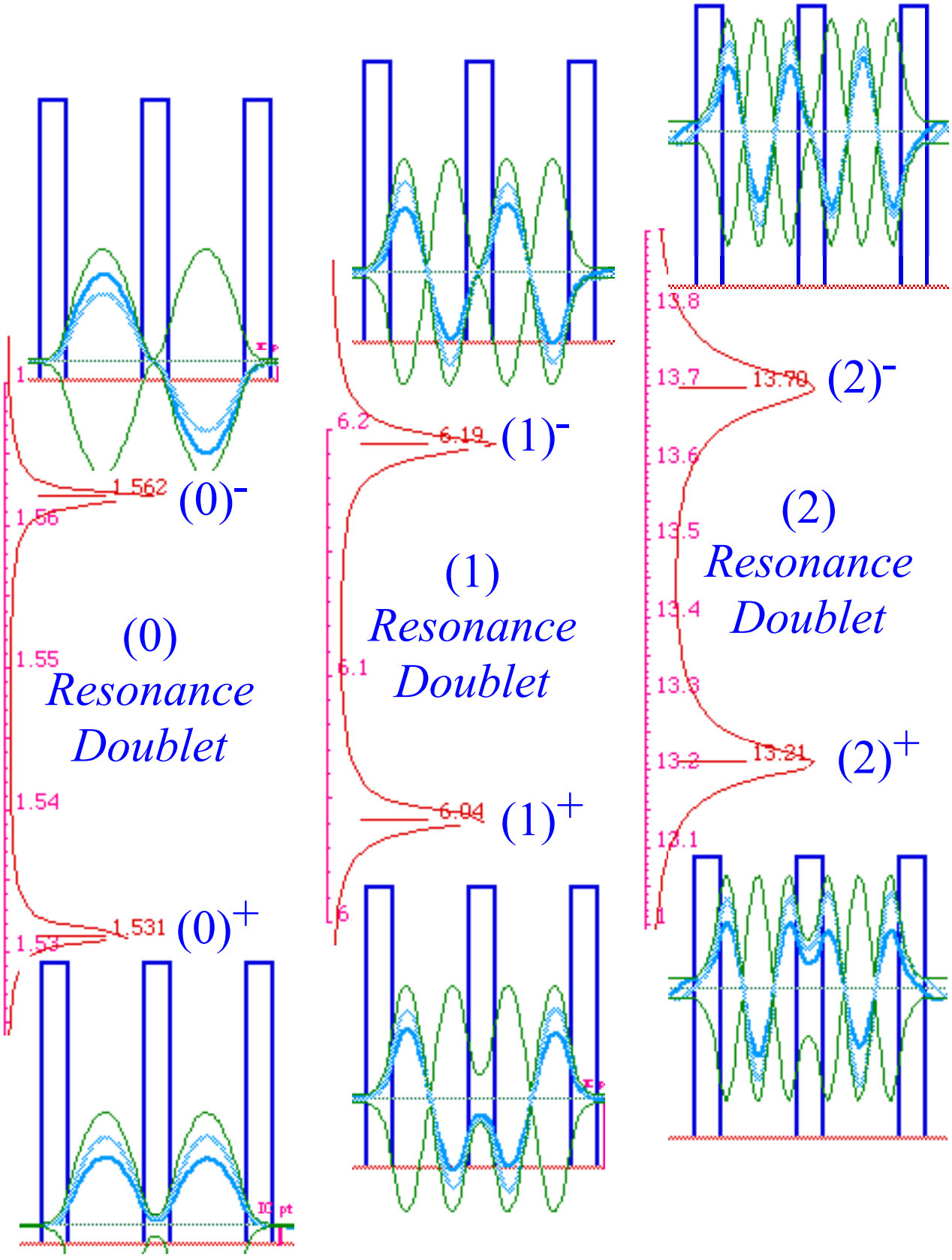

Fig. 14.1.11 Lowest three triple-barrier double-well resonance parity doublets

Instead, C_2 symmetry lets us whittle that number down to three: the even and odd doublet frequencies $\omega(n^+)$ and $\omega(n^-)$,which are eigenvalues of a bilateral symmetry (*B*-type) Hamiltonian (14.1.5).

$$\omega(n^+) = H(n) - S(n) , \qquad \omega(n^-) = H(n) + S(n) ,$$

and a single decay rate $\Gamma(n^+) = \Gamma(n) = \Gamma(n^-)$. The latter gives the *Half-Width-at-Half-Maximum (HWHM=Γ(n))* of either doublet peak. Fig. 14.1.11 shows that peaks within each pair have nearly the same width but that this width grows quasi-exponentially for increasing quantum number *n* of higher energy doublets. The parameter *S(n)* is the *half-splitting (HS = S(n))* of the *n-th* doublet. It also grows quasi-exponentially with *n*.

Finally, *H(n)* is the *center of gravity (CG = H(n))* of the *n-th* doublet and evidently it is, once again, remarkably close to the bound-state eigenvalue of a well of the same width *(W=1.5)* and height *(V=25)* but with walls of infinite thickness *(L=∞* for the "high-security prison.") even though the walls used here are relatively flimsy *(L=0.5)*. The *CG* of resonance *(0)* in Fig. 14.1.11 is

$$H(0) = (1.562 + 1.531)/2 = 1.5465$$

This is close to the bound state eigenvalue *E(0) = 1.547* derived earlier.

Note that maximum amplitudes of transmission peaks are all 100% $(|C_{11}(\omega(n^{\pm}))|=1)$ for resonances in C_2 symmetric potentials (Prove this!). So amplitude coefficients *c(n)* are all equal to the decay rate Γ*(n)* and the $c(n^{\pm})$ parameters are not needed here.

Fig. 14.1.11 shows that doublet peak half-width Γ*(n)=HWHM* grows more rapidly with increasing quantum number *n* than doublet half-splitting *S(n)=HS* , so that when *n=2* or *3* the two peaks are practically rubbing shoulders. In other words, the decay or "probability leakage" rate *2Γ(n)* increases relative to the transition or "quantum beat" frequency *2S(n)*. Each successively higher doublet resonance, if excited uniformly, will behave more and more like a rusty old damped pendulum. Finally, it becomes "over damped" when *Γ(n)>S(n)*, and the beat oscillation dies before it can complete a single cycle.

The beat frequency *2S(n)* is determined mainly by the central barrier which, as it becomes thicker, reduces coupling between the two wells. If, instead, the central barrier is made thinner and finally removed altogether, the doublet splitting *2S(n)* increases until it is comparable to the spacing between the neighboring *CG=H(n)* values. Finally, the double-well spectrum becomes that of a single well.

Plots of $(2^{\pm})$ doublet resonance wavefunctions in Fig. 14.1.12 show that the two waves differ appreciably only in the middle barrier. The lower energy (2^+) channel wave is, at the moment shown,

$$\Psi^{2+}(x,0) = C \cosh \kappa_+ x + i\, S \sinh \kappa_+ x. \quad (-L/2 < x < L/2) \qquad (14.1.13a)$$

Its hyperbolic cosine part is much larger than the imaginary hyperbolic sine part.(*C>>S*) At an equivalent moment of time, the (slightly) higher energy (2^-) channel wave inside the barrier is,

$$\Psi^{2-}(x,0) = S \sinh \kappa_- x - i\, C \cosh \kappa_- x, \quad (-L/2 < x < L/2) \qquad (14.1.13b)$$

with the hyperbolic sine much larger than the imaginary cosine. (*S>>C*) Ψ^{2-} has a slightly larger κ-value, too, ($\kappa_- > \kappa_+$), but that difference is relatively small. To understand (14.1.13) we view each *channel* wave as combinations of their respective *eigenchannel* waves which were introduced in Sect. 13.3(c).

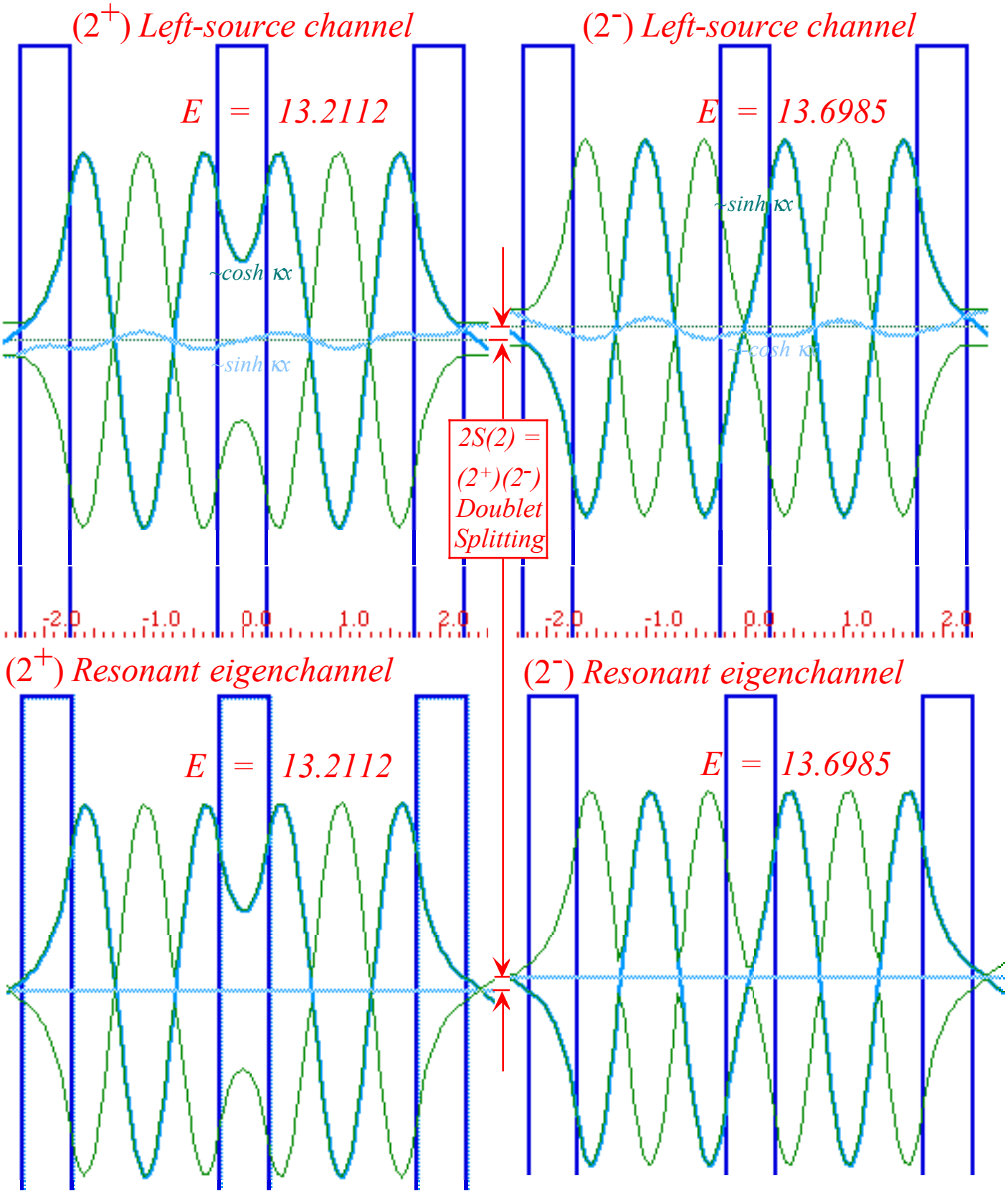

Fig. 14.1.12 (n=2) resonant parity doublet. Channel states have100% transmission. Eigenchannels, none.

Recall that eigenchannels must be standing waves as shown by (13.3.15a-b). A left-source channel wave must be have pure moving wave (*coskx+isinkx*) in the output (right) channel and therefore be a complex *50-50*

combination of eigenchannels. However, the interior parts the channel states, (2^+) or (2^-), are combinations, (14.1.13a) or (14.1.13b), respectively, of interior eigenchannel waves which appear to be anything but *50-50*, in fact one dominates the other as we see now.

In the preceding resonance example there is a pure moving wave in the input (left) channel since transmission happens to be *100%*. To have moving waves (*coskx+isinkx*) on both sides requires equal amounts of both symmetric ("cosine-like") and antisymmetric ("sine-like") eigenchannel wave components in the exterior region. One of the eigenchannel components will be a *resonant eigenchannel* with large amplitude in the interior (well) region while the other component will be a *non-resonant eigenchannel* with a small interior amplitude, just like equations (14.1.13).

The resonant (2^+) and (2^-) eigenchannels are plotted in the lower portion of Fig. 14.1.12, and clearly these account for most of the interior part of (2^+) or (2^-) channel waves. However, each channel wave has a *non-*resonant component that has the *opposite* symmetry with a small interior contribution as plotted in Fig. 14.1.13. The non-resonant plot amplitudes are exaggerated over the resonant ones so the symmetry of small interior standing waves are clearly visible. The non-resonant (2^+) wave is anti-symmetric and the non-resonant (2^-) wave is symmetric; opposite to the resonant waves in Fig. 14.1.12.

This explains why channel waves are slightly lopsided; the asymmetry of (2^+) in Fig. 14.1.11 is not due to numerical error. Current flow requires a non-zero phase lag downstream and all the more so if the current is large compared to interior amplitudes. The required asymmetry is supplied by a nonresonant part, which, for *100%* transmission at a resonant energy, has an exterior amplitude equal but *90°* out of phase with the resonant part of the same energy, but it comes with a small interior wave, too.

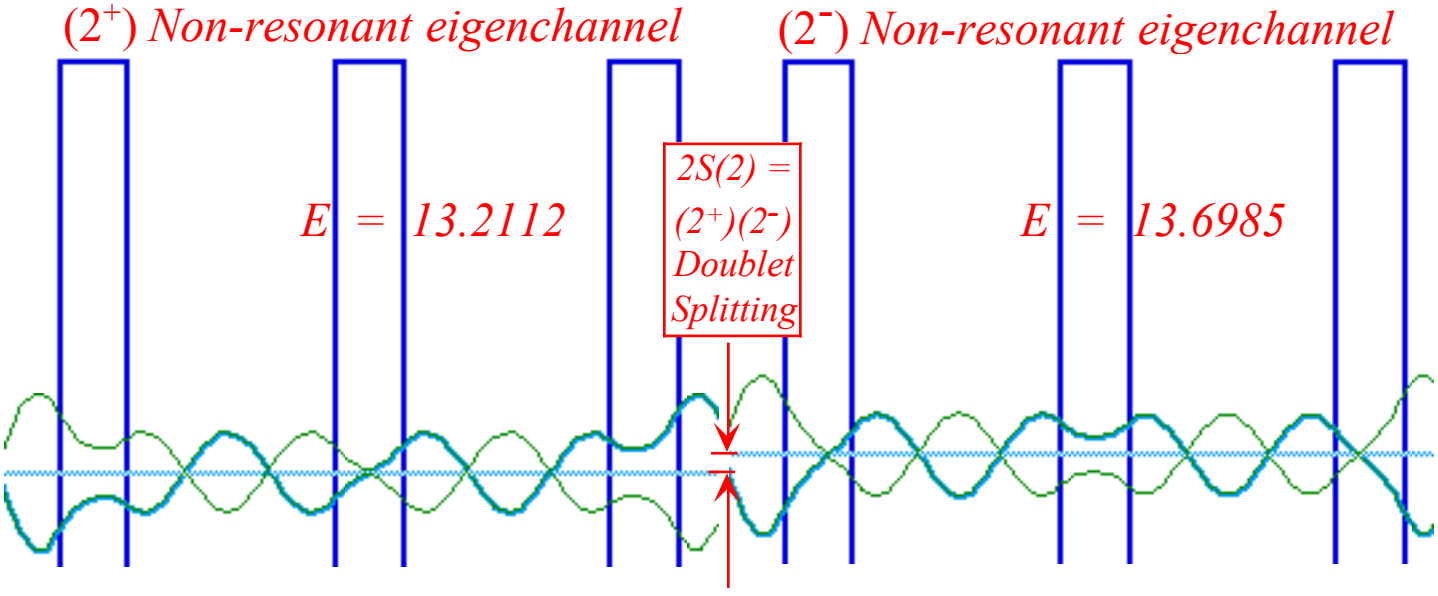

Fig. 14.1.13 (n=2) non-resonant eigenchannel parity doublet. Amplitude is exaggerated over Fig. 14.1.12.

Recall that eigenchannels have a full *SU(2)* freedom. The preceding figures display only the eigenchannels referred to origin at the center of C_2 symmetry as, for example, in (13.3.39). However, any combination of the resonant and non-resonant eigenchannels is an eigenchannel, too, having the same energy but

a different reference origin. Experimentally, a range of eigenchannels is obtained by dragging the source or initial condition (*IC*) point along the *x*-axis for half a wavelength or by scanning the initial *R* or *L* phase component through π or varying the *a*-parameter, as in Fig. 13.3.3. Only the waves shown in Fig. 14.1.12 and 13 have a pure C_2 odd or even (±) parity. Others are "non-descript" symmetry like some examples of (2^+) waves shown below.

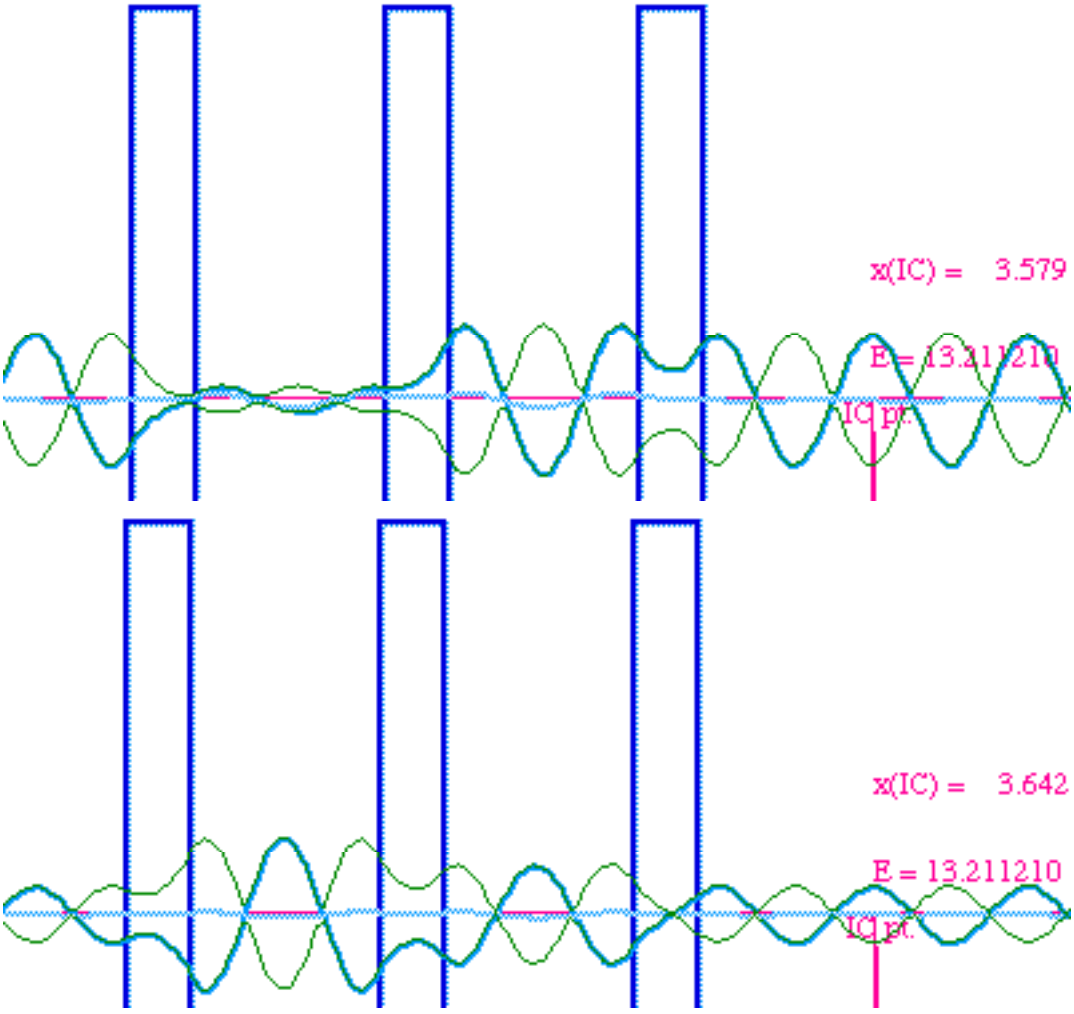

Fig. 14.1.14 Generic (2^+) eigenchannel wave combinations of indefinite parity.

The doublet coupling and splitting parameter *S(n)* is determined by the middle barrier, but the decay rate Γ*(n)* is determined mostly by the outer walls. Making them thicker on the outside (increasing *L* without changing the middle barrier L_M or the well width *W*) makes the resonance peaks thinner and the resonances stronger without appreciably altering either the *CG* or *HS* values. Infinitely thick exterior walls give singlet-level bound states shown in Fig. 14.1.2 and 3. Each one is a resonant eigenchannel wave, the winning partner of a doublet level. The losing and forgotten partner is the non-resonant eigenchannel wave which is squeezed out to the infinite *L*. Old states don't die, they just fade away!

(1) Breaking C_2 symmetry

It is important to see how the resonances described so far are sensitive to the presence or lack thereof of the bilateral *B*-type of C_2 symmetry. As was pointed out in Sec. 10.3, the reduction of *B*-type to *AB*-type and finally to asymmetric-diagonal *A*-type symmetry begins when the diagonal **H**-matrix components $H_{11}=A$ and

$H_{22}=D$ differ by more that the off-diagonal $H_{12}=HS=S$ components. For the lower resonances of the triple-barrier double-well the $S(n)=HS$ parameter is tiny so it doesn't take much diagonal asymmetry to wholly upset this system and thereby spoil its strong resonances and perfect transmission properties.

This is what is seen in Fig. 14.1.15. A tiny perturbation or "bump" at the bottom of the left hand well is enough to almost completely destroy the giant *(n=0)* resonances shown on the left side of Fig. 14.1.11 and reduces its 100% transmission to less than 1%. However, the higher *(n=2)* resonance fares better since its $2S(2)=0.49$ parameter is much larger than $2S(0)=0.031$, and so it is perturbed into only slightly asymmetric combinations. The transmission is still not exactly *100%* but still close to it.

There are many ways to make or break the C_2 symmetry. Adjusting the depth or width of one of the wells or the thickness or height of one of the outer barriers will have the same effects. So will adding a uniform electric field which puts a slope on the entire potential system as shown in Fig. 14.1.16. The latter is an example of the electric Stark splitting. Generally this quickly spoils 100% transmission, too.

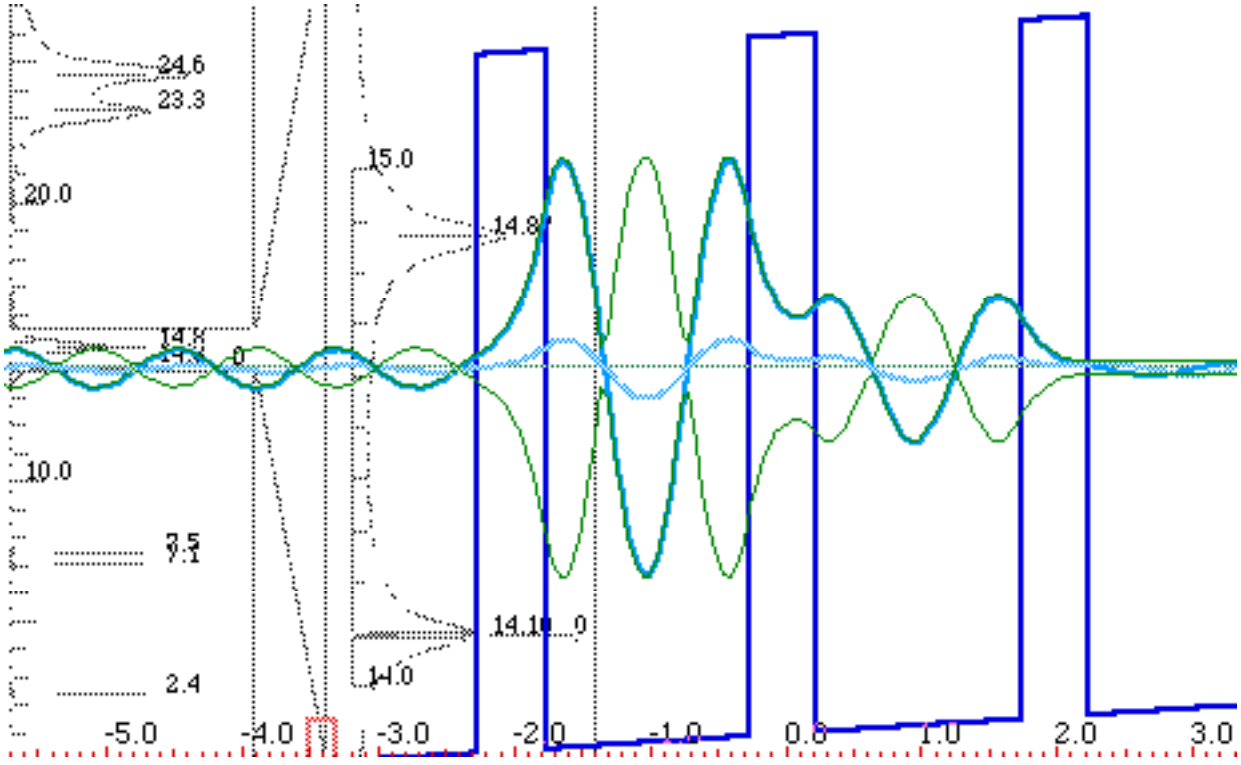

Fig. 14.1.16 Lower state of Stark split (2^+) resonance doublet.

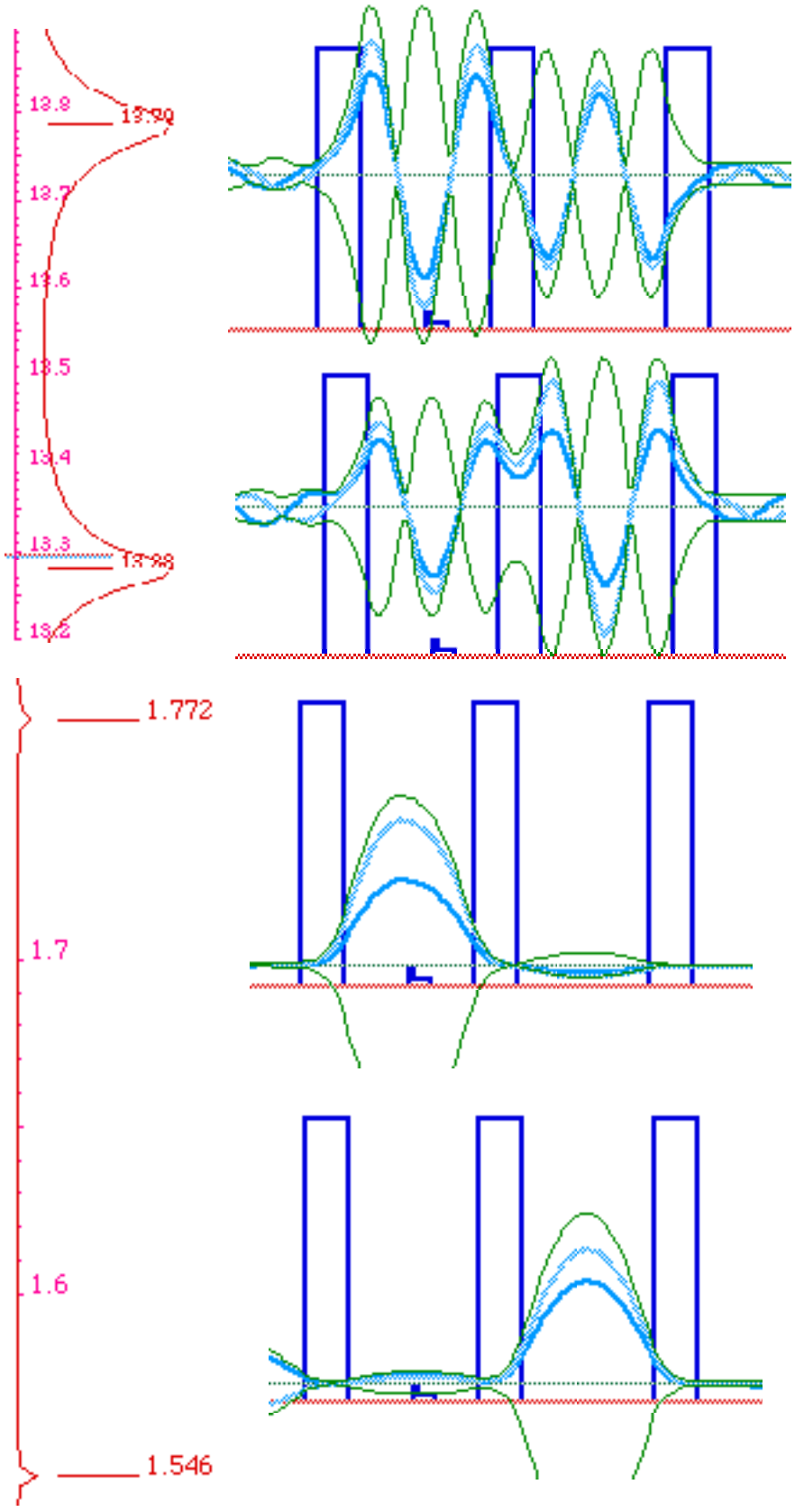

Fig. 14.1.15 Small symmetry breaking ruins (n=0) resonance doublet and slightly perturbs (n=2).

(2) Accidental degeneracy

If one well is detuned sufficiently it may come back into resonance, but with the next higher level of the neighboring well. In the Fig. 14.1.17 the *(n=0)* state of the left well has been pushed up so it is in resonance with the *(n=1)* wave of the right hand well. This is called an *accidental degeneracy* even if it is no accident. (It takes some effort to pull this off!) The difficulty with this kind of "accident" is that none of the other levels are likely to also have degenerate mates since no over-riding symmetry is present.

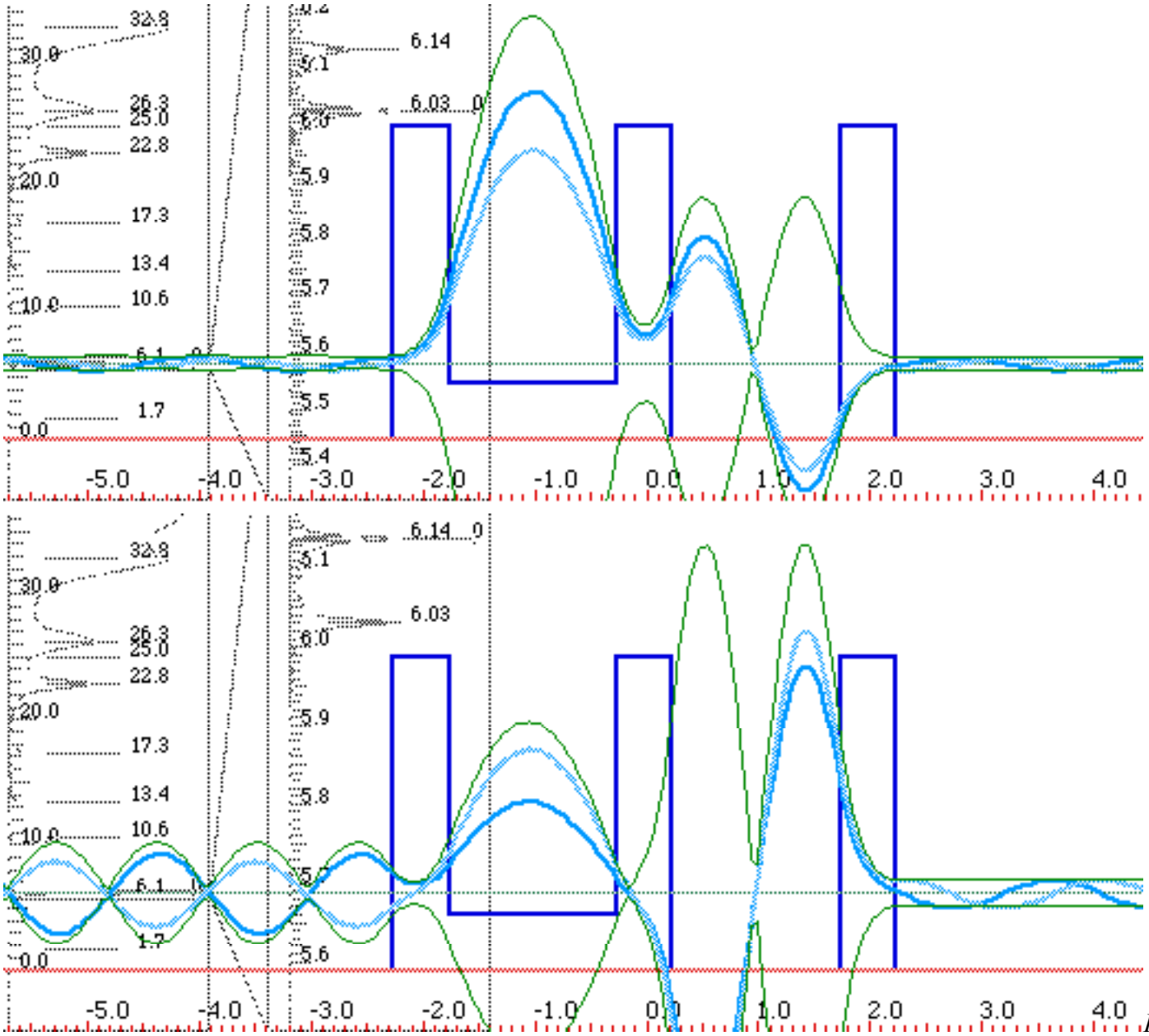

Fig. 14.1.17 Extreme symmetry breaking brings (n=0) resonance up to (n=1).

(e) Multiple humps or wells

By increasing the number N of identical potential wells strung together between $N+1$ barriers, as in Fig. 14.1.18, we find transmission spectra that begin to resemble band spectra of crystalline solids.

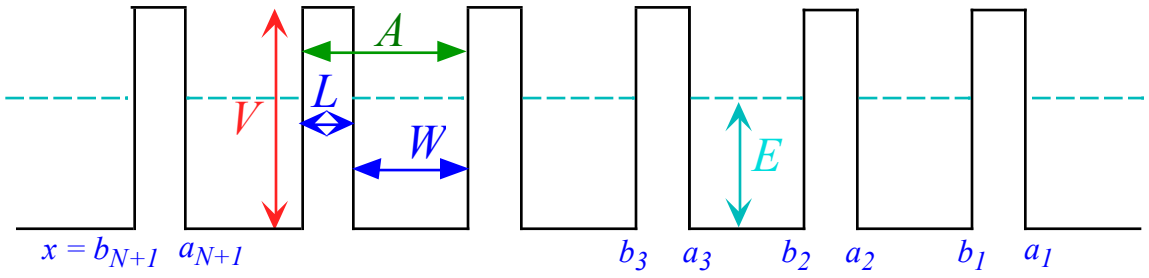

Fig. 14.1.18 (N+1)-barrier (N)-well potential

Each of the $N+1$ barriers has a C-matrix which enters a product to make the overall C-matrix.

$$C^{N+1\,barrier} = C^{[N+1]}\cdots C'\cdot C = \begin{pmatrix} e^{ikL}\chi^* & -ie^{-ik(a_{N+1}+b_{N+1})}\xi \\ ie^{ik(a_{N+1}+b_{N+1})}\xi & e^{-ikL}\chi \end{pmatrix}\cdots\begin{pmatrix} e^{ikL}\chi^* & -ie^{-ik(a_2+b_2)}\xi \\ ie^{ik(a_2+b_2)}\xi & e^{-ikL}\chi \end{pmatrix}\cdot\begin{pmatrix} e^{ikL}\chi^* & -ie^{-ik(a_1+b_1)}\xi \\ ie^{ik(a_1+b_1)}\xi & e^{-ikL}\chi \end{pmatrix} \quad (14.1.17a)$$

As in (14.1.11) the parameters for ($E<V$) are $k = \sqrt{(2E)}$, $\kappa = \sqrt{(2V-2E)}$, and $\sinh 2\beta = (\kappa^2-k^2)/(2k\kappa)$,

$$\chi = \cosh \kappa L - i \sinh 2\beta \ \sinh \kappa L, \ \text{and:} \ \xi = \cosh 2\beta \ \sinh \kappa L, \qquad (14.1.17a)$$

and for ($E>V$) they are $\ell = \sqrt{(2E-2V)}$, and $\cosh 2\alpha = (\ell^2+k^2)/(2k\ell)$ from (13.3.33).

$$\chi = \cos \ell L + i \cosh 2\alpha \ \sin \ell L, \ \text{and:} \ \xi = \sinh 2\alpha \ \sin \ell L. \qquad (14.1.17b)$$

(1) N=3: Coupled pendulum model

With three barriers the transmission peaks derived from (14.1.17 a and b) for ($E<V$) come in triplets. The lowest triplet and associated channel wavefunctions are shown in Fig. 14.1.19. The triplet eigensolutions can be approximated by treating each the three wells as one of three base states $\{|1\rangle,|2\rangle,|3\rangle\}$ in a three-by-three tunneling Hamiltonian eigenvalue equation. It is analogous to three pendulums in a line.

$$\mathbf{H}|\varepsilon_k\rangle = \begin{pmatrix} H & -S & 0 \\ -S & H & -S \\ 0 & -S & H \end{pmatrix}\begin{pmatrix} \langle 1|\Psi\rangle \\ \langle 2|\Psi\rangle \\ \langle 3|\Psi\rangle \end{pmatrix} = \varepsilon_k \begin{pmatrix} \langle 1|\Psi\rangle \\ \langle 2|\Psi\rangle \\ \langle 3|\Psi\rangle \end{pmatrix} = \varepsilon_k |\Psi\rangle \qquad (14.1.18)$$

We solve this by a trick where (14.1.18) is embedded (twice) in a C_8 matrix equation. (Recall Fig. 12.2.6.)

$$\mathbf{K}|\Psi\rangle = \left(\begin{array}{cccc|cc|cc} H & -S & & & & & & -S \\ -S & H & -S & 0 & & & & \\ & -S & H & -S & & & & \\ & 0 & -S & H & -S & & & \\ \hline & & & -S & H & -S & & \\ \hline & & & & -S & H & -S & 0 \\ & & & & & -S & H & -S \\ -S & & & & & 0 & -S & H \end{array}\right)\left(\begin{array}{c} \langle 0|\Psi\rangle \\ \hline \langle 1|\Psi\rangle \\ \langle 2|\Psi\rangle \\ \langle 3|\Psi\rangle \\ \hline \langle 4|\Psi\rangle \\ \hline \langle 5|\Psi\rangle \\ \langle 6|\Psi\rangle \\ \langle 7|\Psi\rangle \end{array}\right) = \varepsilon \left(\begin{array}{c} \langle 0|\Psi\rangle \\ \hline \langle 1|\Psi\rangle \\ \langle 2|\Psi\rangle \\ \langle 3|\Psi\rangle \\ \hline \langle 4|\Psi\rangle \\ \hline \langle 5|\Psi\rangle \\ \langle 6|\Psi\rangle \\ \langle 7|\Psi\rangle \end{array}\right) = \varepsilon|\Psi\rangle \qquad (14.1.19)$$

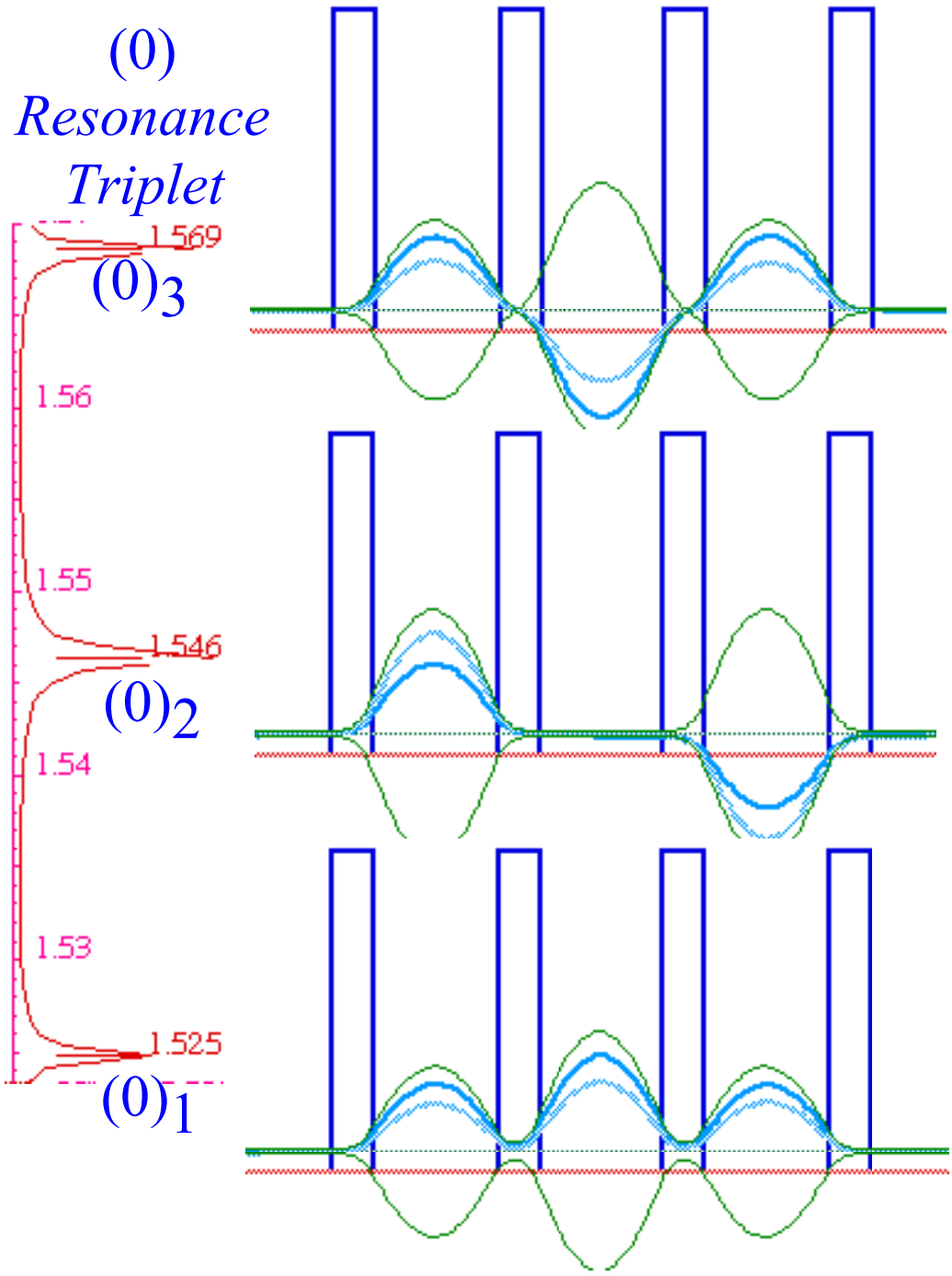

Fig. 14.1.19 Lowest triple-well resonance triplet.

The trick works because the C_8 superset problem has three solutions which make the components $\langle 0|\Psi\rangle$ and $\langle 4|\Psi\rangle$ equal to zero. Then (14.1.18) is solved by the 3-by-3 part of (14.1.19) using the general C_N solutions for $N=8$ from (9.3.5a-e) and discarding five symmetric (cosine-like) eigensolutions. Three sine-like eigensolutions from (9.3.5g) for $(m=1, 2, 3)$ remain for which $\langle 0|\Psi\rangle = 0 = \langle 4|\Psi\rangle$.

$$\varepsilon_m = H - 2\,S\cos k_m a = H - 2\,S\cos(2\pi\, m/8) \qquad (14.1.20a)$$

The k_m–eigenvectors, listed in (9.3.5b) as ±moving waves, need to be combined into sine waves.

$$\langle +k_m| = \left(\begin{array}{c|ccc|ccc} 1 & e^{ik_m a} & e^{2ik_m a} & e^{3ik_m a} & e^{4ik_m a} & e^{-3ik_m a} & e^{-2ik_m a} & e^{-ik_m a} \end{array} \right) / \sqrt{8} \qquad (14.1.20b)$$

$$\langle -k_m| = \left(\begin{array}{c|ccc|ccc} 1 & e^{-ik_m a} & e^{-2ik_m a} & e^{-3ik_m a} & e^{4ik_m a} & e^{3ik_m a} & e^{2ik_m a} & e^{ik_m a} \end{array} \right) / \sqrt{8} \qquad (14.1.20c)$$

$$k_m a = 2\pi\, m / 8 = 0,\ \pi/4,\ \pi/2,\ 3\pi/4, \text{ and } \pi \qquad (14.1.20d)$$

The desired standing sine wave eigenvectors are the difference between the two moving wave states.

$$\langle s_m| = \left(\langle +k_m| - \langle -k_m| \right) / i\sqrt{2}$$
$$= \left(\begin{array}{c|ccc|ccc} 0 & \sin k_m a & \sin 2k_m a & \sin 3k_m a & 0 & -\sin 3k_m a & -\sin 2k_m a & -\sin k_m a \end{array} \right) / 2$$

The 3-well resonances use only the components *m=1*, *2*, and *3* of the (renormalized) sine eigenvectors

$$\langle \varepsilon_m| = \left(\begin{array}{ccc} \sin k_m a & \sin 2k_m a & \sin 3k_m a \end{array} \right) / \sqrt{2} = \left(\begin{array}{ccc} \sin\frac{\pi\, m}{4} & \sin\frac{2\pi\, m}{4} & \sin\frac{3\pi\, m}{4} \end{array} \right) / \sqrt{2}\ , \qquad (14.1.21a)$$

for *m = 1, 2,* and *3*, which give the three eigensolutions using (14.1.20a).(See also Fig. 14.1.20 below.)

$$\varepsilon_m = H - 2\,S \cos(\pi\ m/4)\ . \qquad (14.1.21b)$$

$$\begin{array}{ll} \langle \varepsilon_1| = \left(\begin{array}{ccc} 1 & \sqrt{2} & 1 \end{array} \right) / 2 & \varepsilon_1 = H - \sqrt{2}S \\ \langle \varepsilon_2| = \left(\begin{array}{ccc} 1 & 0 & -1 \end{array} \right) / \sqrt{2} & \varepsilon_2 = H \\ \langle \varepsilon_3| = \left(\begin{array}{ccc} 1 & -\sqrt{2} & 1 \end{array} \right) / 2 & \varepsilon_3 = H + \sqrt{2}S \end{array} \qquad (14.1.21c)$$

Using the value of the tunneling or splitting parameter *S(0) =0.031/2= 0.0155* from the splitting of the double well in Fig. 14.1.11 we can estimate the splitting of the triple-well to be $S(0)\sqrt{2} = 0.0219$ for the $(0)_m$ triplet. This is close to the *0.022* splitting found in the exact calculation plotted in Fig. 14.1.19. A minor swindle of a missing factor-of-two is due to our cutting open a C_N -loop as discussed later.

The trick here is to embed a linear *N*-fold symmetric system (Here *N=3*.) into a circular *2N+2*-fold or C_{2N+2} system (Here, an octagonal C_8 ring.) and then discard all but the *N* solutions that are sine-like. This approximation depends on the linear *N*-fold system having exterior amplitudes which are small enough that they can be modeled by zeros of the *2N+2*-fold sine-wave nodes.($\langle 0|\Psi\rangle = 0 = \langle N+1|\Psi\rangle$)

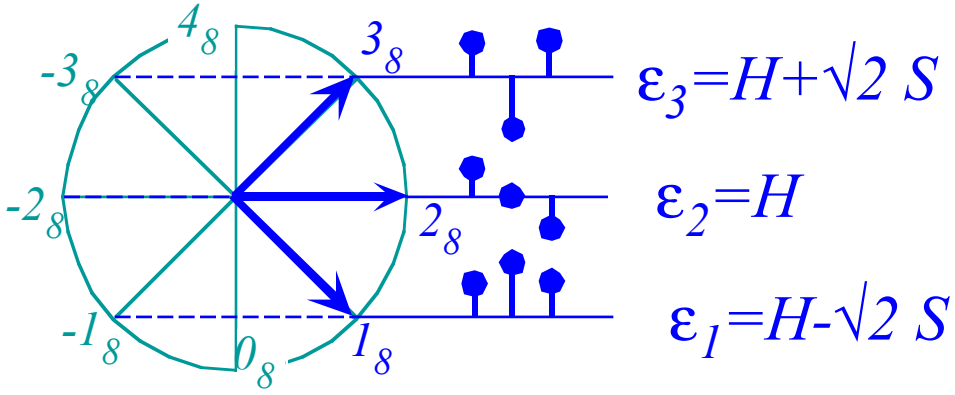

Fig. 14.1.20 Approximate "coupled pendula" C_8 tunneling model for triple-well resonance triplets.

So, it shouldn't be surprising that the approximation is best in strong resonance where huge interior resonance waves dwarf the exterior (input-output) wavefunctions, but it deteriorates for higher resonances which "escape" easily. High-security prisons make this model look better!

Compare the *(1)* doublet parameter *S(1) = 0.15/2=0.075* in Fig. 14.1.11 to the *(1)* triplet splitting of *6.23-6.12=0.11* in Fig. 14.1.21. This is close to the approximate prediction of *√2 (0.75) = 0.106* but, perhaps, not quite as close as the comparison between the lower energy *(0)* resonances made previously.

However, For the *(1)*-triplet the most symmetric *(1, √2, 1)/2=|(1)$_1$⟩* state comes out on top instead of being the lowest as in the *(0)*-triplet while the *(1, -√2, 1)/2=|(1)$_3$⟩* is lowest. This is as it should be since waves with more nodes are always higher energy, so tunneling parameter *S(1)* the opposite sign of *S(0)*.

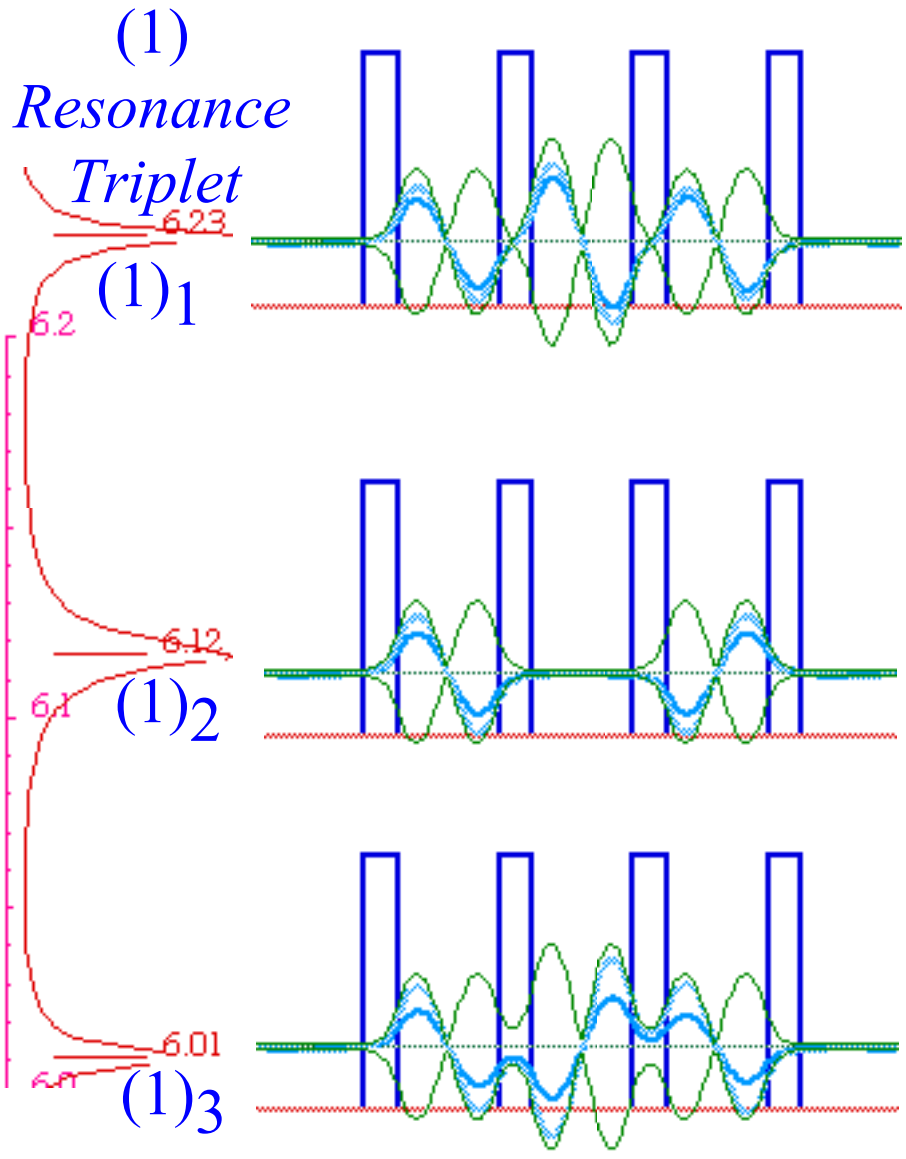

Fig. 14.1.21 Next lowest triple-well resonance triplet.

Another problem with the simple model (14.1.21) is it does not predict *splitting asymmetry*, that is, that ε_1-ε_2 isn't quite equal to ε_2-ε_3 . We could say that the evanescence or tunneling parameter *S(n)* varies with energy within each triplet (while changing sign between them), but this sort of "hand-waving" defeats the elegance of the model. Sec. 14.2 has some ways to improve multplet or band modeling and explain quantitatively how the tunneling and phase vary.

(2) Forbidden gaps

With $N= 4, 5,...$ wells or more, the resonances begin to resemble bands of N peaks spaced out more or less according to the C_{2N+2} eigenvalues from (14.1.20a) with allowed $m = 1, 2, ...N$, only.

$$\varepsilon_m = H - 2\,S\cos k_m a = H - 2\,S\cos(2\pi\, m/(2N+2)) \qquad (14.1.20a)_{repeated}$$

In between each of these bands of peaks lies a "no-man's-land" of energy values that give a disappointing transmission probability which falls off exponentially with the length NA of the potential region. The technical name for a "no-man's-land" is *a forbidden energy gap*.

An example of some pitiful waves trying to penetrate through the first forbidden gap in an $N=4$ system is shown in Fig. 14.1.22. The top wave (Fig. 14.1.22(a)) is only detuned by $\Delta E=0.1$ from the powerful *(0)* resonance band around $E=1.547$. (Recall Fig. 14.1.11 and 19.) Transmission is essentially zero, but it's enormous compared to that of the plot below in which the detuning is doubled to $\Delta E=0.2$. Further detuning attenuates the wave so badly that even the first well has no visible life. Dead on arrival!

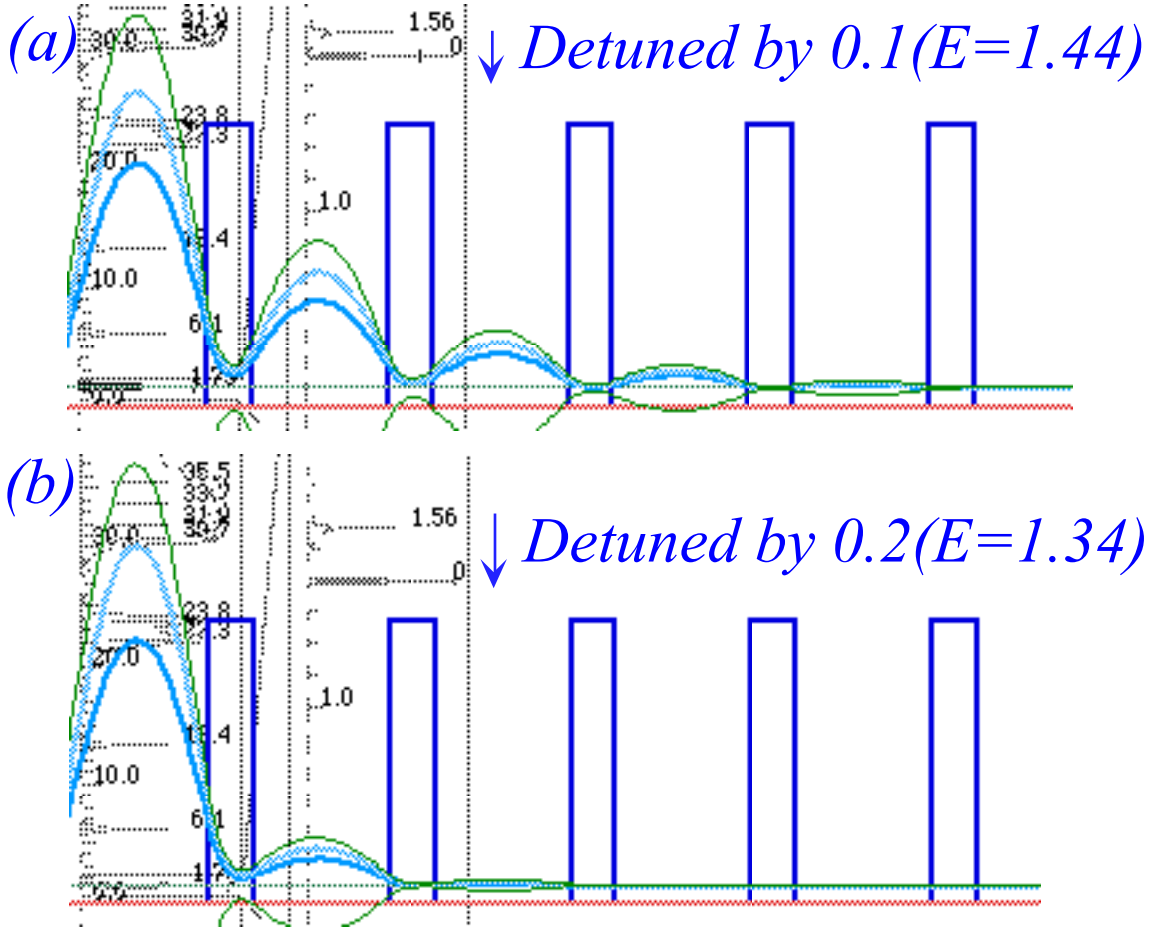

Fig. 14.1.22 Examples of waves dying from detuning into a "forbidden gap" below a resonance band.

(f) Comparing bound *versus* resonant energies

Before beginning energy band theory, let us do a precise comparison of bound-state well energy values with those of resonance peaks. Consider first the well bound-state eigenvalues in Fig. 14.1.23. The energies are listed both from top and bottom while their units are related to standard *mks* units, or, the more appropriate nano-technology *Å(eV)s* units

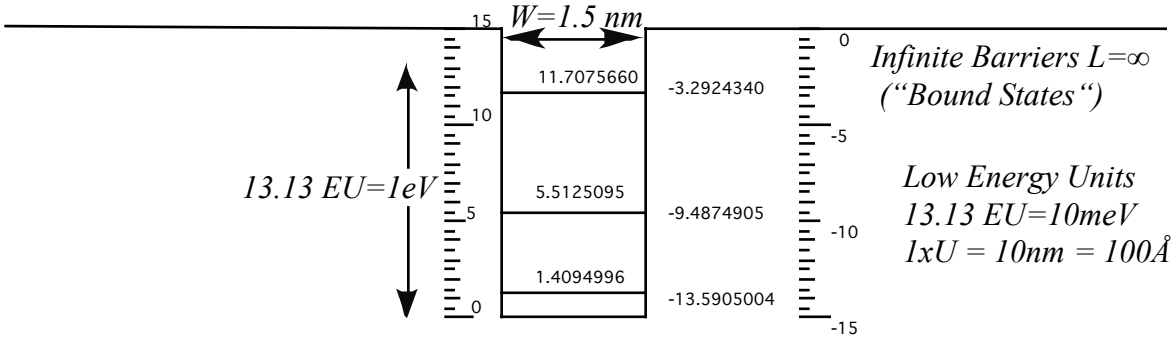

Fig. 14.1.23 Width W=1.5 Square well *with Potential Depth V=15.0EU.*

It is interesting to compare the bound energies to resonance values for wells of the same potential depth *V=15EU* and width *W=1.5 nm*, but varying outer wall thickness . Three examples, varying from thin wall *(L=0.5)* to thick wall *(L=2.0)*, are shown in Fig. 14.1.24.

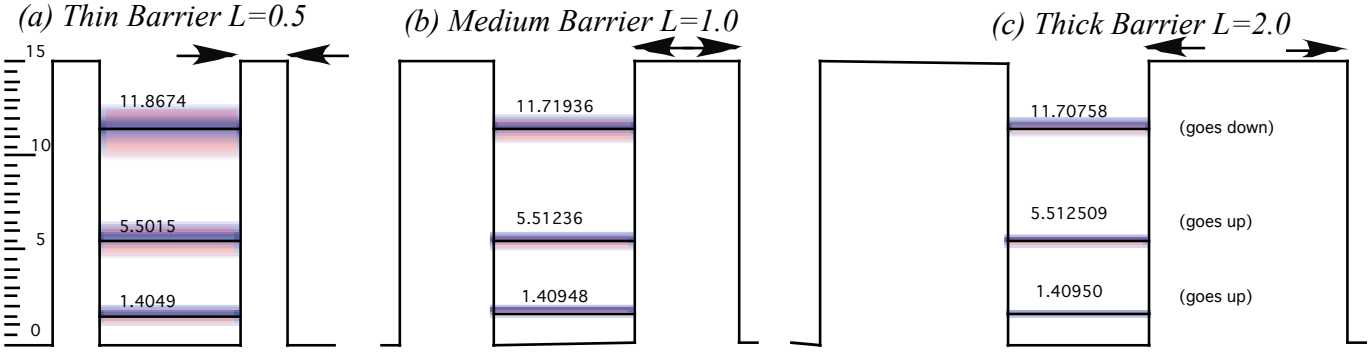

Fig. 14.1.24 Width W=1.5 Resonance wells *with Potential Depth V=15.0EU and varying wall thickness*.

The resonance values in Fig. 14.1.24 are quite close approximations to the "exact" bound-state energies in Fig. 14.1.23 in each case, and they become closer as the outer walls become thicker. The lower resonance values rise slightly as the wall becomes less penetrable, but surprisingly, perhaps, the highest one drops. The variation of energy is complicated by the mixing of resonant and non-resonant eigenchannels. For thick wall and low energy, the bound state wave will approach that of the resonant eigenchannel wave while the non-resonant eigenchannel wave becomes more and more excluded. However, for thin walls, the overlap between the two increases as shown in the discussion of Fig. 14.1.12 and Fig. 14.1.13. Then, their mixing becomes an important part of the energy equation.

Next we compare the case of double-wells. The bound state double-well eigenvalues for this example are dispalayed in Fig. 14.2.25. Note that the doublet centers are quite close to the corresponding singlet values in Fig. 14.1.23. The separating barrier length is *L=0.5 nm*.

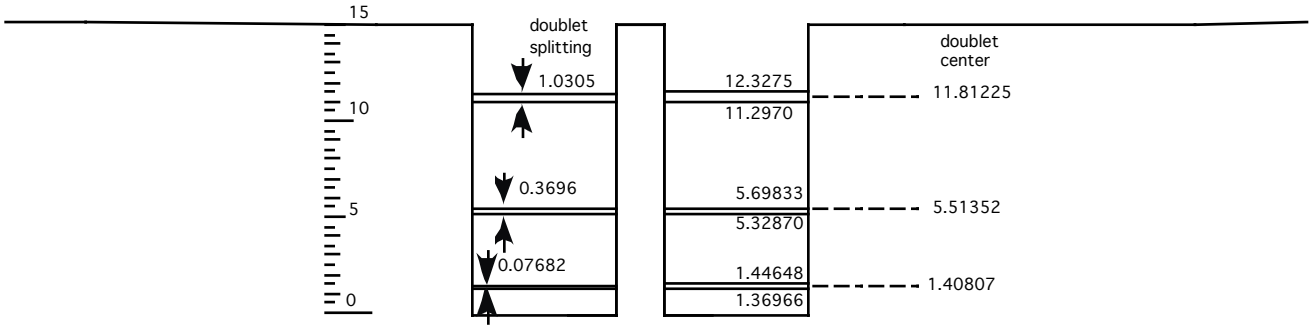

Fig. 14.1.25 Double-well bound state doublets.

In Fig. 14.1.26 below, the doublet bound-state energies above may be compared to resonance values arising from identical double wells surrounded by more or less penetrable walls of thickness length *L=0.5 nm* for Fig. 14.1.26a and *L=1.0 nm* for Fig. 14.1.2b.

(a) 3-Humps Make Double Well *(b) Double Well With Thicker Outside Barrier*

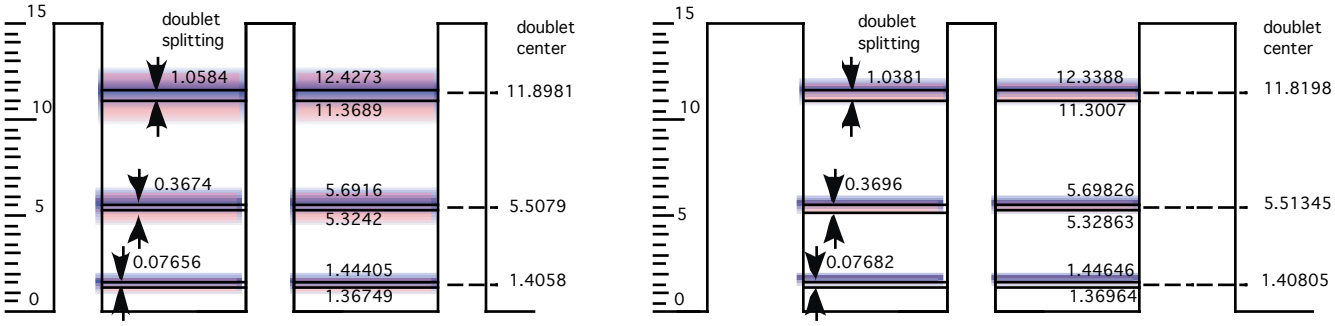

Fig. 14.1.26 Double-well resonance doublets. (a) Thin outer walls (L=0.5 nm), (b) Thick outer walls (L=1.0 nm),

Again, there is a slight downshift of the lower resonances while the highest pair rise slightly. Also, the doublet splitting rises more for the highest doublet particularly in the case of thinner walls. Interaction between resonant and non-resonant eigenchannels is enhanced by having closely spaced doublet energy values.

14.2 Allowed bands: Kronig-Penney Conditions

Forbidden waves like the ones shown in Fig. 14.1.22 get killed because each application of a barrier *C*-matrix gives right and left wave amplitudes *(R', L')* with magnitudes that are products by some factor *F* with the amplitudes *(R, L)* going into that *C*-matrix. The result is an unstable geometric or exponential ($\sim e^{Fx}$) growth or decay and that kills transmission or propagation. If a wave in a forbidden energy gap fails to pass a few barriers, what chance has it in a real crystal with trillions of such barriers? When a crystal says a wave energy is "forbidden" it means it! Fuggedaboutit! Get out'a here!

To see what allows wave propagation we focus on one *C*-matrix factor from the chain (14.1.17).

$$\begin{pmatrix} R' \\ L' \end{pmatrix} = \begin{pmatrix} e^{ikL}\chi^* & -ie^{-ik(a_1+b_1)}\xi \\ ie^{ik(a_1+b_1)}\xi & e^{-ikL}\chi \end{pmatrix} \cdot \begin{pmatrix} R \\ L \end{pmatrix} \qquad (14.2.1)$$

The output wave $\psi'(x)$ and input wave $\psi(x)$ are the following by definition. (Recall Fig. 14.1.5.)

$$\psi'(x) = R'e^{ikx} + L'e^{-ikx}\,, \qquad \psi(x) = Re^{ikx} + Le^{-ikx}. \qquad (14.2.2)$$

Now let's force propagation by demanding that the output wave and its derivative be the same at point $x=A = L + W$ after each barrier-well as it was at the starting point $x=0$. This is a little too strict, but surely if each unit of a lattice puts out the same initial conditions for its wave, then the wave can exist everywhere in the whole system with the same amplitude. That would be perfectly periodic propagation.

So our "strictly periodic" demands take the following forms.

$$\begin{aligned} &\psi'(0) = \psi(A) \quad \text{implies} \quad R' + L' = Re^{ikA} + Le^{-ikA}\,, \\ &\frac{d}{dx}\psi'(0) = \frac{d}{dx}\psi(A) \quad \text{implies} \quad R' - L' = Re^{ikA} - Le^{-ikA}\,. \end{aligned} \qquad (14.2.3a)$$

Solving gives $R'=Re^{ikA}$ and $L'= L\,e^{-ikA}$. Putting this into *C*-relation (14.2.1) gives

$$\begin{pmatrix} R' \\ L' \end{pmatrix} = \begin{pmatrix} e^{ikL}\chi^* & -ie^{-ik(a_1+b_1)}\xi \\ ie^{ik(a_1+b_1)}\xi & e^{-ikL}\chi \end{pmatrix} \cdot \begin{pmatrix} R \\ L \end{pmatrix} = \begin{pmatrix} Re^{ikA} \\ Le^{-ikA} \end{pmatrix} = \begin{pmatrix} e^{ikA} & 0 \\ 0 & e^{-ikA} \end{pmatrix} \begin{pmatrix} R \\ L \end{pmatrix} \qquad (14.2.3b)$$

So the following matrix *M* has only zero eigenvalues.

$$M \cdot \begin{pmatrix} R \\ L \end{pmatrix} = \begin{pmatrix} e^{ikL}\chi^* - e^{i2kA} & -ie^{-ik(a_1+b_1)}\xi \\ ie^{ik(a_1+b_1)}\xi & e^{-ikL}\chi - e^{-i2kA} \end{pmatrix} \cdot \begin{pmatrix} R \\ L \end{pmatrix} = \begin{pmatrix} 0 \\ 0 \end{pmatrix} \qquad (14.2.4a)$$

Setting its determinant to zero and using unimodularity ($|\chi|^2-\xi^2=1$) yields the following conditions.

$$\begin{aligned} \det M &= \left(e^{ikL}\chi^* - e^{ikA}\right)\left(e^{-ikL}\chi - e^{-ikA}\right) - \xi^2 \quad = 0 \\ &= |\chi|^2 - e^{ikL}\chi^* e^{-ikA} - e^{-ikL}\chi e^{ikA} + 1 - \xi^2 = 0 \qquad (14.2.4b) \\ \mathrm{Re}\left(e^{ik(L-A))}\chi^*\right) &= 1 = \mathrm{Re}\left(e^{ikW}\chi\right) \end{aligned}$$

where $W=A-L$ is the width of the well and $L=A-W$ is the barrier length. Using (14.1.17a-b) this becomes

$$\left.\begin{aligned} &(for\ E>V): \quad \cos kW\,\cos \ell L - \cosh 2\alpha \sin kW\,\sin \ell L \\ &(for\ E<V): \quad \cos kW \cosh \kappa L + \sinh 2\beta \sin kW \sinh \kappa L \end{aligned}\right\} = 1 \qquad (14.2.5a)$$

The last equations are called the *Kronig-Penney band conditions*. These are plotted in Fig. 14.2.1 for the potential with $L=0.5$, $W=1.5$. Observed bands are located inside the regions between $\mathrm{Re}(e^{ikW}\chi)=\pm 1$. Indeed, the *1* in (14.2.5a) needs to be relaxed to ± 1, or, better, to $\cos(2\pi m/N)$ for C_N bands.

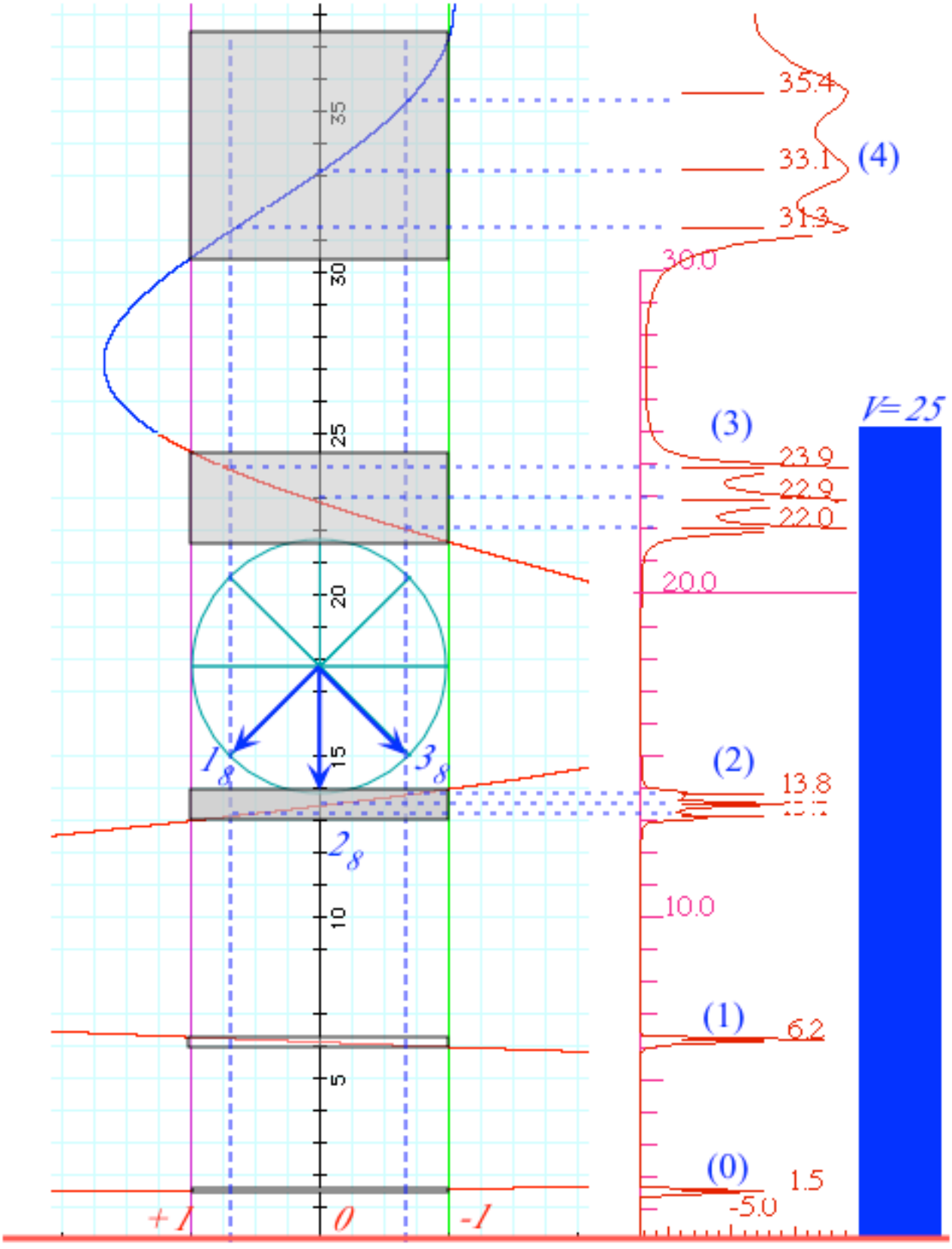

Fig. 14.2.1 Kronig-Penney functions and related 3-well-4-barrier triplet resonance bands.

It is too strict to demand that the wave recover its original form after *each* well-barrier. If instead we demand ψ recover only after passing *N* well-barriers for some integer *N*, then ψ needs to pick up an equal phase ϕ = *2π m/N* from each barrier so it recovers after *N*. This gives the following.

$$\left.\begin{array}{l} (for\ E>V):\quad \cos kW\ \cos \ell L - \dfrac{2E-V}{2\sqrt{E\left(E-V\right)}} \sin kW\ \sin \ell L \\ (for\ E<V):\quad \cos kW \cosh \kappa L + \dfrac{V-2E}{2\sqrt{E\left(V-E\right)}} \sin kW \sinh \kappa L \end{array}\right\} = \cos\phi \qquad (14.2.5b)$$

where rational units are used for energy.

$$\phi = m\frac{2\pi}{N}\ , \qquad k=\sqrt{2E}\ , \qquad \ell=\sqrt{2\left(E-V\right)}\ , \qquad \kappa=\sqrt{2\left(V-E\right)}\ . \qquad (14.2.5c)$$

The values of the phase shift ϕ = *2π m/N* are indicated as angles from the horizontal in Fig. 14.2.1. The middle member of the triplet experiences a phase shift of ϕ =π/2.

An exactly zero phase shift is not possible with a line of wells because the wavefunction needs to taper off as it approaches the right or left hand walls of a linear *N*-well system. Only a circular or periodic (Bohr-like) C_N ring (discussed next) can afford to have a zero or π phase shift. The tapering can be visualized by imagining an enveloping sine wave for each of the *N*-well multiplets. The longest allowed sine wave has one wave length enveloping the entire *2N+2*-well double-ring C_{2N+2} system. That amounts to a half wave over the space occupied by *N+1* wells, or the smallest possible phase shift of

$$\phi_{min} = \pi /(N+1) \qquad (14.2.6)$$

That is an angle $\phi_{min} = \pi /4$ or *45°* for the *N=3*-well system in Fig. 14.2.1.

The enveloping sine shapes are seen more clearly as *N* increases as shown in Fig. 14.2.2 below.

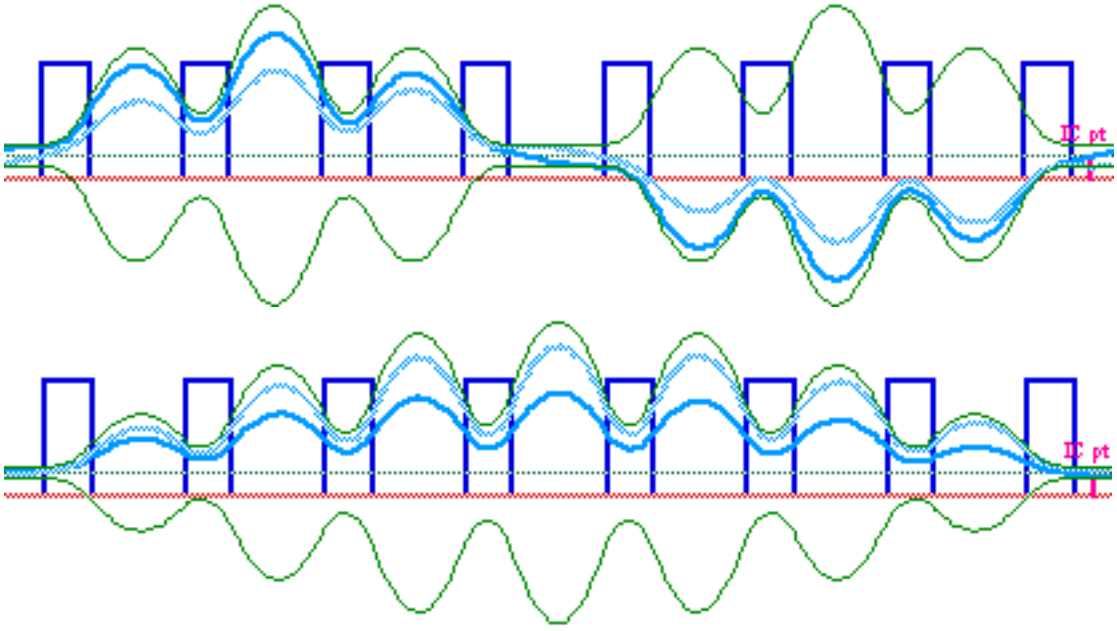

Fig. 14.2.2 Lowest two members of the (0)-septet resonance band in a linear 7-well system..

The highest allowed phase shift is just ϕ_{min} short of π. An example of such a wave is shown if Fig. 14.2.3 is the highest energy member of the *(0)*-octet whose lowest waves are shown above Fig. 14.2.2.

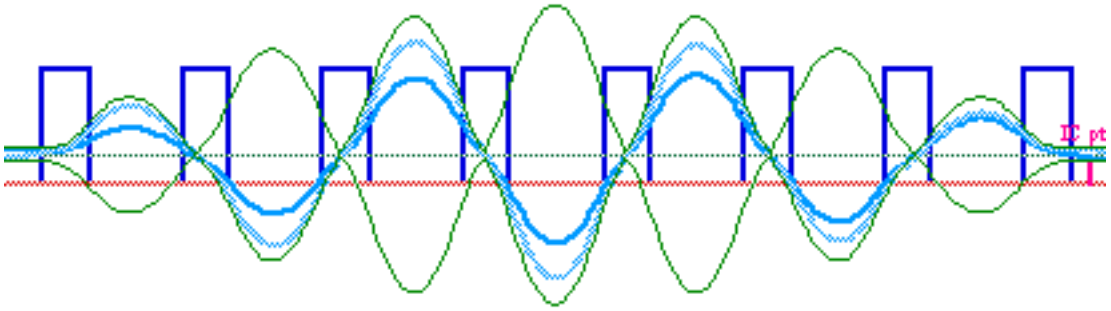

Fig. 14.2.3 Highest member of the (0)-septet resonance band in a linear 7-well system..

The slope and curvature of the Kronig-Penney (KP) functions inside the limits ±1 determine the band or multiplet structure. Only when the KP functions approach straight lines do the simple coupled pendulum model formulas (14.1.20) become precise. This happens for the lower resonances of deep wells. But for the upper resonances, and certainly for the *E*-above-*V* waves, the KP functions undergo ever longer oscillations barely exceeding the ±1 limits. At higher *E* the bands begin to dominate the spectrum while the gaps become narrow, quite the opposite of the lower spectral regions where the reverse is true.

Even in the lower *E* regions there are observable effects of the curved KP functions some of which were mentioned before. One of these is the asymmetry of the multiplet splitting. For the even multplets (0), (2), (4),... the KP function curves upward going left to right in Fig. 14.2.1. This will generally make the upper members of each multiplet have slightly greater splitting than the lower ones. The odd (1), (3),..multiplets have their order reversed since the KP function curves upward right to left so again it is the higher energy multiplet members that experience phase and energy enhancement.

(a) Band structure for large-N periodic lattices

As more and more identical well-barriers are strung together, the resonance multiplets in the transmission spectrum acquire more and more peaks. In the limit of an infinite number of barriers (Perhaps, it is wiser to just say *many* barriers.) a sharp band structure emerges that is characteristic of the shape of the individual well-barrier. Fig. 14.2.4 shows a summary of the transmission spectra for the *W=1.5* well and *L=0.5* barrier of height *V=25* for *N=1, 2, 3, 4,* and *5* wells such as have been studied in the preceding sections. As *N* increases the band structure begins to emerge from the individual well structure. The forbidden gaps become more forbidden and the allowed bands become more allowed. This is particularly noticeable in the energy regions above the barrier where the multiplet splitting is large and can be seen filling up the allowed bands as *N* increases. Recall that the minimum phase ϕ_{min} of (14.2.6) decreases with *N* so that the outer multiplets can more closely approach the Kronig-Penney band edges.

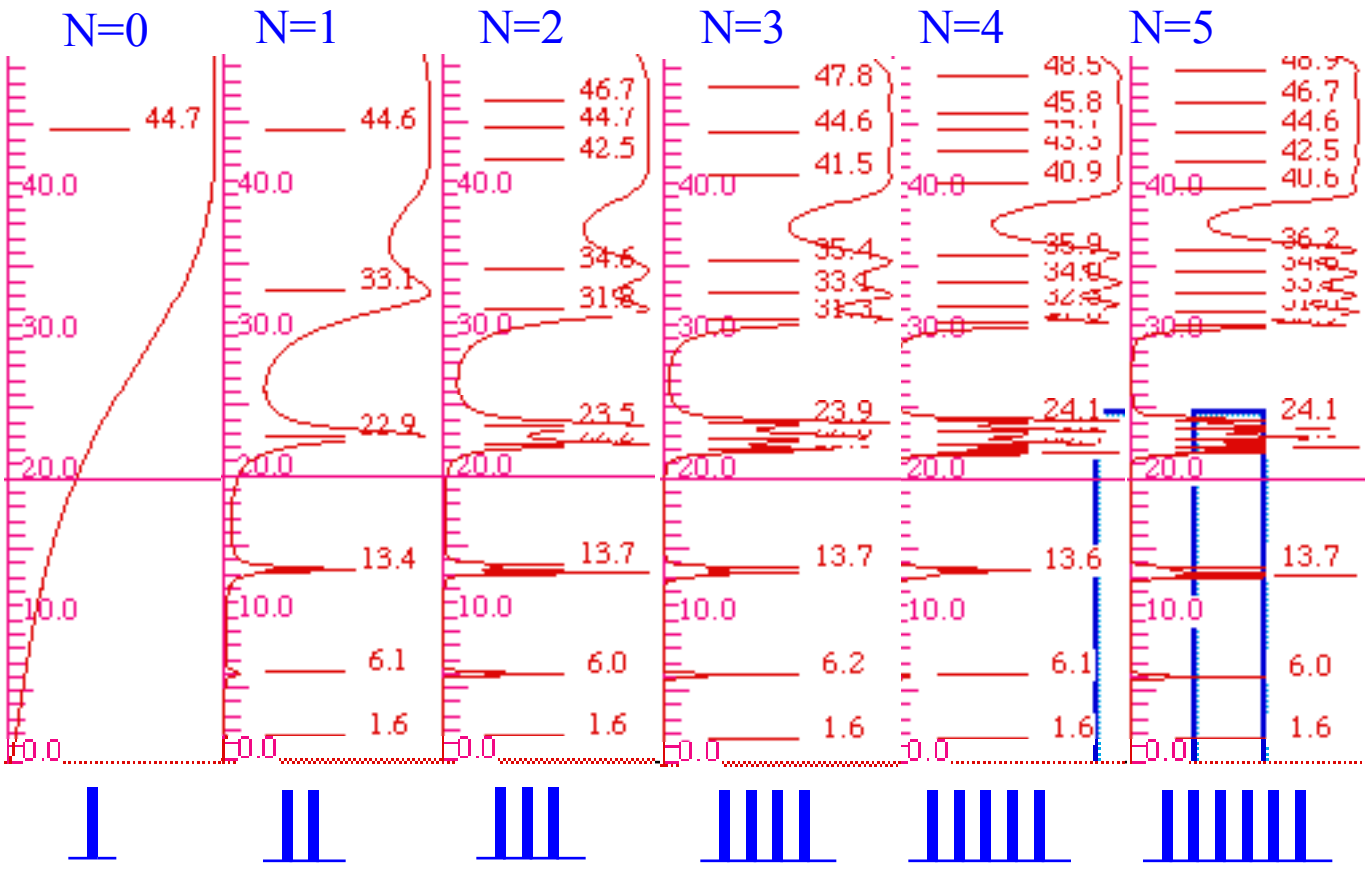

Fig. 14.2.4 Transmission resonance spectrum becoming more like band structure as N increases.

The variation of KP band edges with barrier height V is plotted in Fig. 14.2.5 for the $W=1.5$ well and $L=0.5$ barrier ending with barrier height $V=25$. This is a plot for the limit of large N and the allowed regions are shaded while the forbidden gaps are blank. The KP bands for $V=25$ from Fig. 14.2.1 are related to the V-plot in Fig. 14.2.5.

Note that KP band edges pass over the barrier top without any disruption. Without the diagonal line representing $E = V$, it would be practically impossible to tell where the barrier top was located. This is in contrast to the disruption we noted in going above the barrier top for a square well as in Fig. 13.2.2. The difference is that the latter disruption resulted from going from a discrete bound state system to a wholly different continuum topology. Here, the energy is always in a continuum though that continuum is divided into allowed and forbidden band regions by the presence of a periodic lattice potential.

The lower allowed bands *(0), (1), (2),*...become extremely narrow as V increases. Deeper wells make the tunneling splitting parameters *S(0), S(1), S(2),*...exponentially small. For large V the lower curves in Fig. 14.2.5 become lines that approximate the discrete square well eigenvalues of Fig. 13.2.5-6 and approach the infinite-well energies discussed in Section 12.1a. This is shown more clearly a few pages ahead in Fig. 14.2.7 and Fig. 14.2.11.

(next page) *Fig. 14.2.5 Band structure as V increases for 0<V<25. (W=1.5 well ,L=0.5 barrier)*

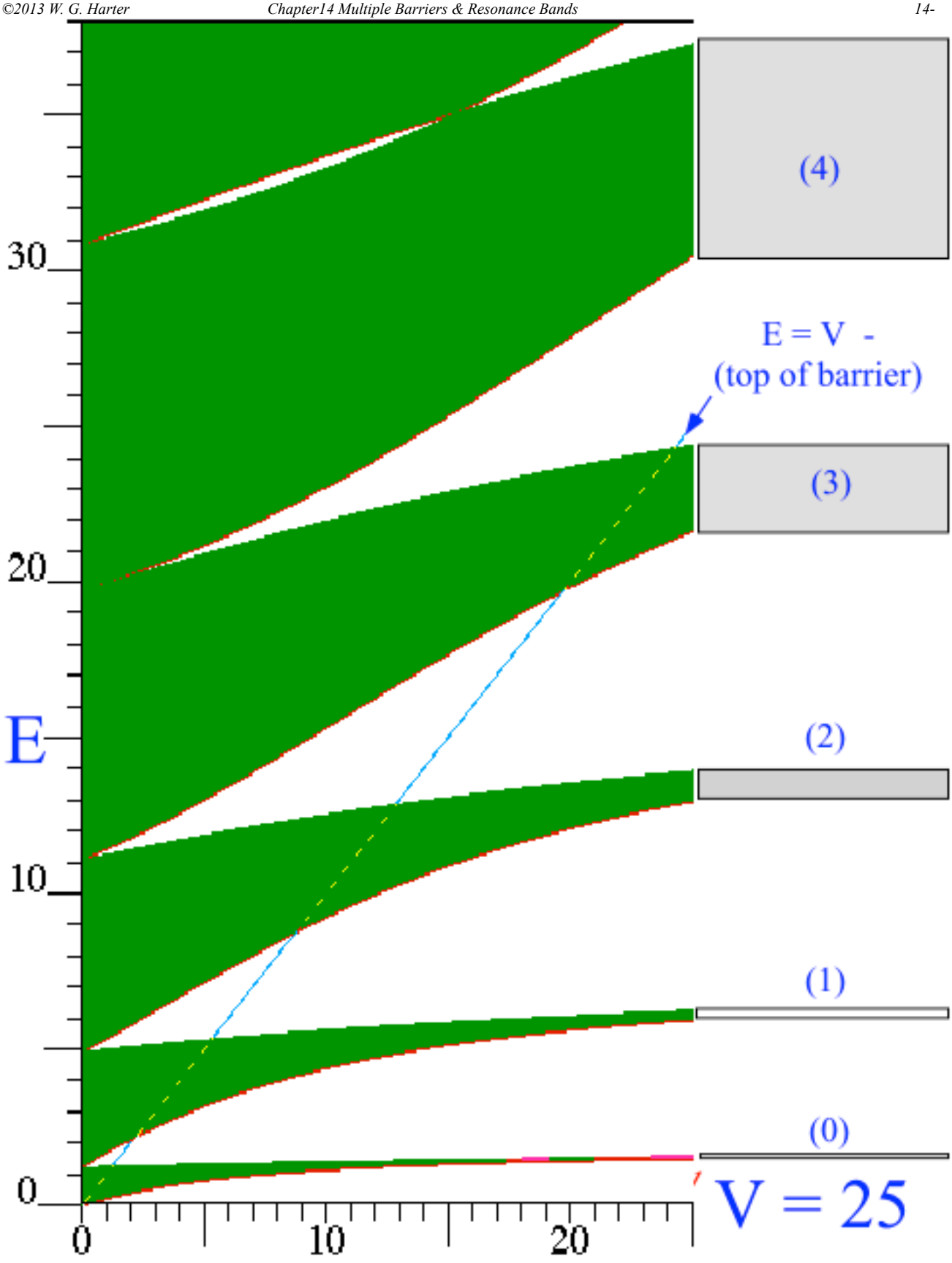
(4)
E = V -
(top of barrier)
(3)
(2)
(1)
(0)
E
V = 25
30
20
10
0
0
10
20

(b) Bohr and Bloch lattices and band structure

The splitting and crossing of the Kronig-Penney bands can be understood by imagining the *N*-well lattices to be wrapped around a cylinder so that the left hand barrier is identical to the right hand one. Some examples are shown in Fig. 14.2.6. If we close a loop with *periodic boundary conditions* we get a discrete Bohr-like or Bloch-like spectrum as described in Sec. 9.3. (Recall Fig. 9.3.3.) As *N* increases the cylinder gets larger so as to maintain the dimensions *W* and *L* of each well and the barrier, respectively. Also, as *N* increases, the discrete energy level density increases as discrete bands become continuous.

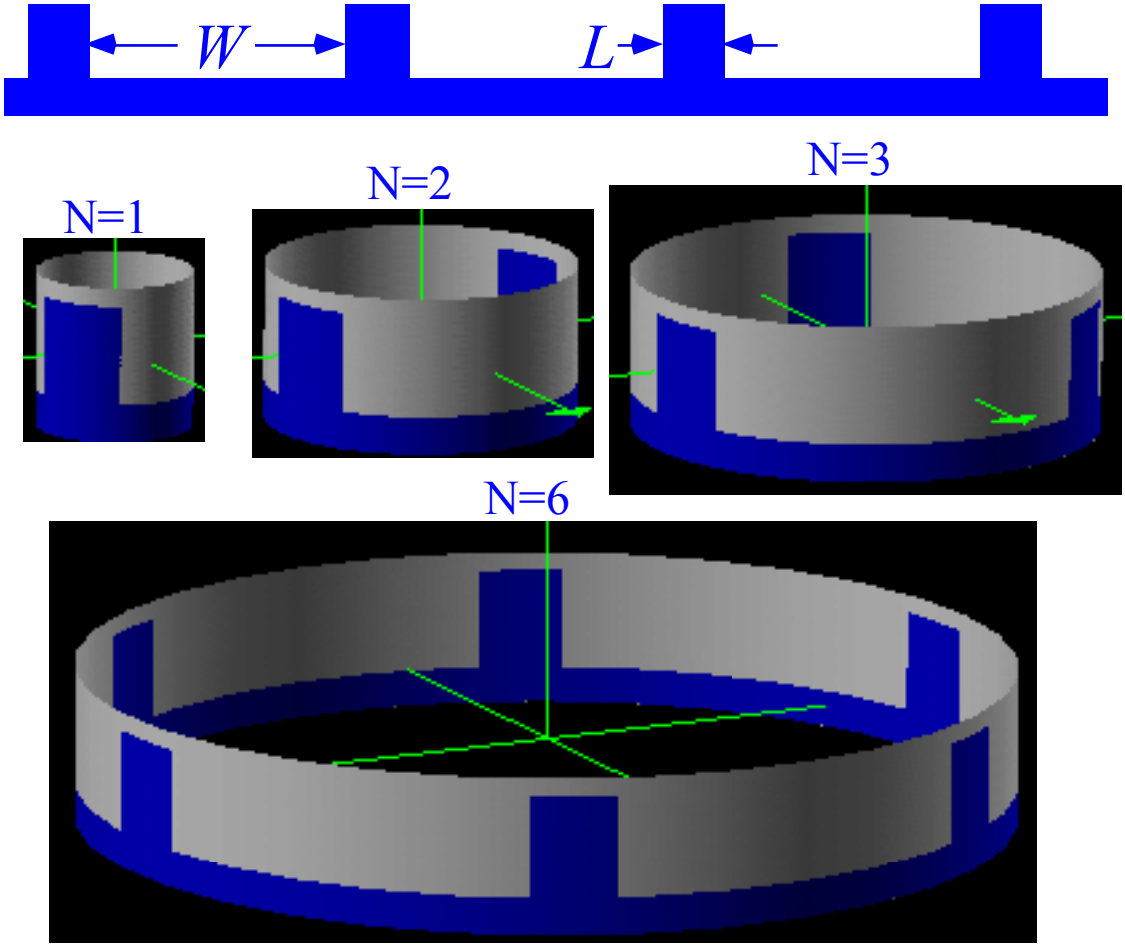

Fig. 14.2.6 Periodic lattices for Bohr-Bloch orbital problem. (W=1.5 well ,L=0.5 barrier)

A key unit of distance is the lattice length constant $A = L + W$. For reasons that will soon be seen, we take twice this distance to be a fundamental *(υ=1)* Bohr wavelength of the *N=2* ring.

$$\lambda_{Bohr} = 2A = 2W + 2L \qquad (14.2.7)$$

(This would be exactly one <u>half</u> wavelength per well lattice spacing *A*.) The resulting Bohr wavevector is

$$k_{Bohr} = \frac{2\pi}{\lambda_{Bohr}} = \frac{\pi}{A} = \frac{\pi}{W + L} \qquad (14.2.8)$$

The energy of such a unit quantum (υ=*1*) Bohr orbital in the absence of a potential *V* is (Recall 12.2.11.)

$$\varepsilon_1^{Bohr}(A)=\frac{\hbar^2}{2M}k_{Bohr}^2=\frac{\hbar^2}{2M}\frac{\pi^2}{A^2}=\frac{\hbar^2}{2M}\frac{\pi^2}{(W+L)^2} \qquad (14.2.9)$$

Now we will use 10^{-8}m=10nm = 100 Ä units of distance since it is one used in some studies of super-lattices, that is $L = 0.5$ will be 50.0 Ä and $W=1.5$ will be 150 Ä . The resulting lattice spacing constant of A, that is $200A$ Ä or 20nm, would give an energy in the milli-electron Volt (meV) range.

$$\varepsilon_1^{Bohr}(A)=\frac{\hbar^2}{2M}\frac{\pi^2}{A^2}=\frac{\left(1.05\cdot10^{-34}\pi\text{J}\cdot\text{s}\right)^2}{\left(2\cdot9.109\cdot10^{-31}\text{kg}\right)}\frac{10^3\text{meV}}{1.602\cdot10^{-19}\text{J}}\frac{1}{\left(A\cdot10^{-8}\text{m}\right)^2} \qquad (14.2.10a)$$

$$=\frac{3.76\text{meV}}{A^2}\quad (A \text{ in units of } 100\text{Ä})$$

Our favorite lattice constant of $A = L + W = 0.5+1.5 = 2.0$ or 200 Ä gives

$$\varepsilon_1^{Bohr}(2) = 0.94 \text{ meV}. \qquad (14.2.10b)$$

Our rational units, for which $\hbar^2/M = 1$, relate to units of meV by a factor $3.76(2/\pi^2) = 0.762$ from (14.2.10), that is, 10 rational E-units is 7.6meV. In rational E-units the Bohr unit energy for our lattice is

$$\varepsilon_1^{Bohr}(A)=\frac{\pi^2/2}{A^2}=\frac{4.93}{A^2}=1.23 \quad (\text{for: } A=2 \text{ in } 100\text{Äunits}) \qquad (14.2.11)$$

These unit relations are displayed prominently in Fig. 14.2.7 which shows more detail of the KP band picture first plotted in Fig. 14.2.5. Of particular note is the band splitting which occurs at the following quantum Bohr energies (in rational units).

$$\varepsilon_\upsilon^{Bohr}=\left(\upsilon_2\right)^2 E_{Bohr}(A)=1.23\left(\upsilon_2\right)^2 \quad (\text{for: } A=2 \text{ in } 100\text{Äunits}) \ , \qquad (14.2.12)$$

Here each non-zero Bohr quantum number $\upsilon_2 = 1, 2, 3,....$, has two curves splitting out from the extreme left hand side of the plot. These curves are the *Brillouin band boundaries* for bands, each of which contains N energy states, one state for each well in the ring. The very lowest $(\upsilon_2=0)$ curve is the only singlet. The rest are doublet pairs which start out as a basic Bohr $\pm\upsilon_2$-doublets (14.2.12) for zero potential barrier height $(V=0)$.

The V-barriers split the Bohr doublets, and for two barriers $(N=2)$ the band boundaries account for the entire spectrum of two $(N=2)$ levels in each "band." The shaded bands of Fig. 14.2.7 disappear since a Bohr ring cannot have a continuum, and for ($N=2$) there are no additional discrete levels inside. (Nothing is left of Alice's Cheshire cat but its smiles! Two "smiles" are seen in the upper portion of Fig. 14.2.7 which we discuss later.) The $(N=2)$ spectrum is entirely composed of single levels which start out on the left hand ($V=0$) side as degenerate Bohr pairs (except for the lone Bohr singlet $(\upsilon=0)$), and only achieve a sort of "re-pairing" for large potential barrier height V, on the right hand side of the figure.

However, lower "re-paired" levels on the right hand side of Fig. 14.2.7 are nearly degenerate. The "re-pairs" are a lot like the "inversion doublets" in a linear double-well. Folding linear $(N=2)$ wells into the $(N=2)$ circular ring potential shown in Fig. 14.2.6 erases the band between the "re-pairs." Circular Bohr-like N-well rings regain linear-well band continua within boundary level pairs as N approaches infinity.

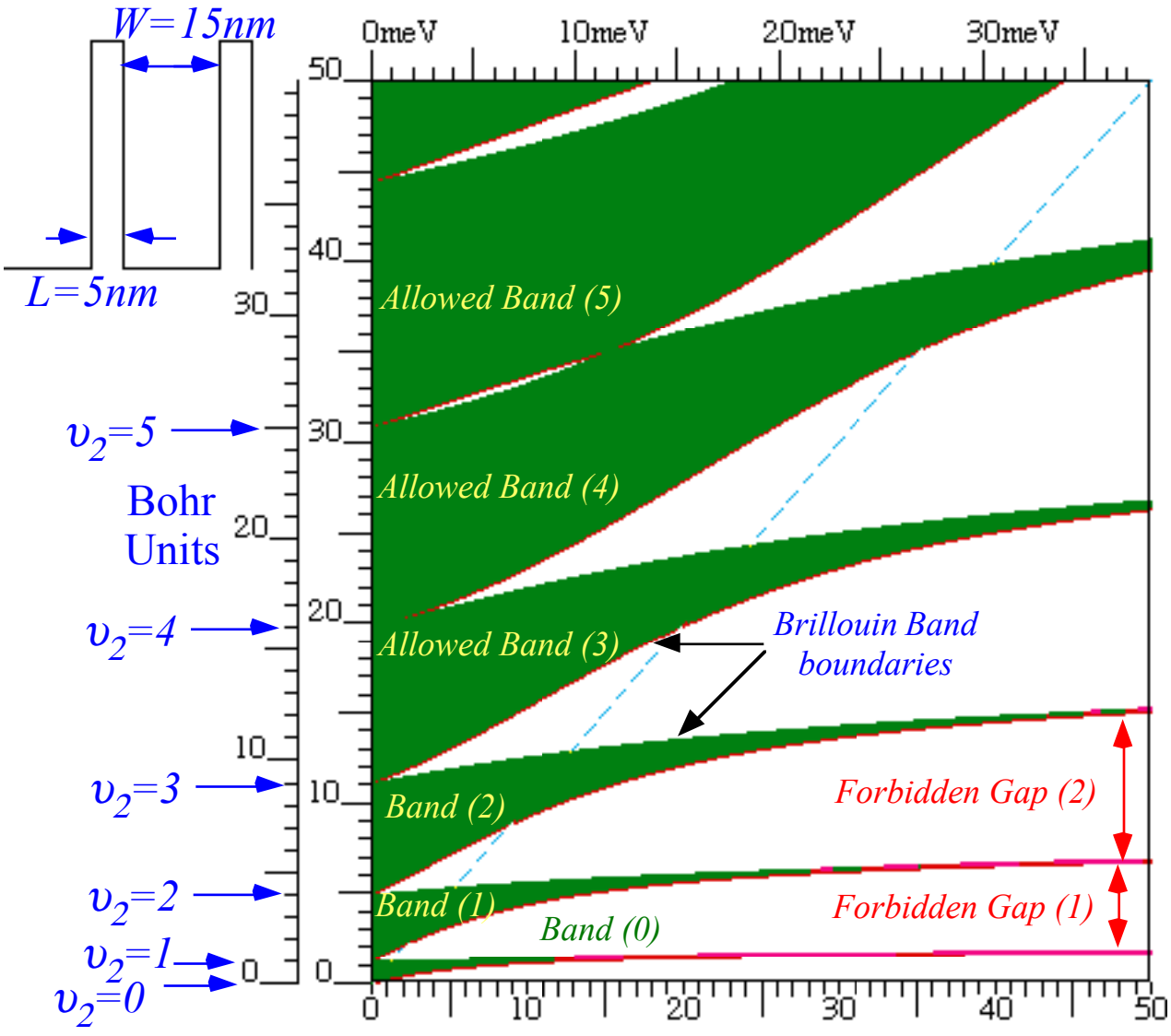

Fig. 14.2.7 Bands vs. V.(W=15nm well ,L=5nm barrier) showing Bohr splitting for (N=2)-ring.

Waves in a circular double wells can couple to each other through either barrier. This should make doublet splitting of linear double wells (which couple only through their middle barrier) about <u>half</u> that of circular wells. The pendulum model (14.1.21) treats a linear double *(N=2)* well *(±)*-wave-doublet as the "sine" parts of circular *(2N+2=6)*-well ring waves 1_6 and 2_6 , and the splitting is, indeed, <u>half</u> the tunneling parameter $S=S(\upsilon)$.

$$\varepsilon(m_6) = H - S\cos 2\pi m/6 = H + (-1)^m(1/2)S \quad \text{for: } m_6 = 1_6 \text{ or: } 2_6 \qquad (14.2.13)$$

This is part of the "minor swindle" alluded to after equation (14.1.21) which can be finally put to rest if we consider the circular $N=6$ potential in Fig. 14.2.6. It is a prototype for the linear $N=2$ potential and is three times as big as the circular $N=2$ ring potential in Fig. 14.2.6. Hence, the $N=6$ ring has room for three times as many Bohr quantum waves as the $N=2$ ring, and we need to triple the Bohr quantum numbers listed in Fig. 14.2.7. Now splittings occur at $\upsilon_6 = 3, 6, 9, 12, 15,..$ and correspond to C_6 *Brillouin Zone band boundaries*. Each band contains six levels labeled by C_6 quantum numbers 0_6, 1_6, 2_6, 3_6, -2_6, and -1_6, deployed according to a

hexagonal projection shown in Fig. 9.3.1 of Chapter 9. Levels $\pm 1_6$ are degenerate as are $\pm 2_6$. In the prototype linear $N=2$ potential we would only keep the sine parts of $\pm 1_6$ and $\pm 2_6$ doublets while discarding the other four. So the linear $N=2$ problem ends up with split doublets like the circular $N=2$ one, but its doublet splitting is only half the Kronig-Penney (KP) band width.

A main difference between the resonance peak spectra of linear N-well systems and the discrete E-levels of prototype circular $(2N+2)$-well systems is that the latter can use the KP band edges while the former never can,... quite. The minimum lattice phase shift of linear wells was $\phi_{min} = \pi/(N+1)$ according to (14.2.6) but a circular wave system can have perfectly periodic waves with exactly zero or exactly π phase shift from well to well. In fact an even-N circular C_N -well system uses all the KP band edges while an odd-N C_N -well system uses half the KP band edges, skipping every other one. This is shown in Fig. 14.2.8 by comparing $N=3$ and $N=6$ ring spectra.

The potentials in Fig. 14.2.8 have V reduced from $V=25$ to $V=5$ so it is easy to see the splitting of even the first (0) band of multiplets. As before in Fig. 14.2.1, the KP function snakes back and forth across the vertical "tracks" left by the phase projections $\cos\phi = \cos m(2\pi/N)$. Intersections of "tracks" with the KP function determine the energy eigenvalues of the multiplets in each band $(0), (1), (2), ...,$ and there will be exactly N energy states per band.

One feature present here that was absent from the linear N-well resonances is the double degeneracy of every energy level that lies inside the ± 1-tracks that define the band edges. This is because right moving waves with positive wavevector $+k_N = +m(2\pi/N)$ are assumed to have the same frequency and phase speed as left-moving waves with reversed wave vector $-k_N = -m(2\pi/N)$. Each such m-pair leads to a *symmetry doublet* E_m *state* that is labeled E_m on the right hand side of the diagrams in Fig. 14.2.8. Pure moving-wave eigenstates are impossible for a linear N-well structure; indeed, we tossed out all the "cosine parts" of the circular prototypes in the linear-coupled-pendulum model. So, there went the "cosine-half" of each doublet. Circular C_N-rings, on the other hand, need both sine and cosine parts to make a complete set of $U(2)$ wave states.

The other "cosine parts" that were discarded from the linear N-well problem are the ones with phase $\phi = 0$ and $\phi = \pm\pi$ which lie right on the $\cos\phi = \pm 1$ tracks that define the band boundaries. These are all singlet (non-degenerate) standing-wave states labeled as *symmetry singlet* A_1, B_1, A_2, *or* B_2, *states*, depending on where they fall on the KP diagram, which fixes their wave symmetry as is sketched below. The letter "A" means "Always-the-same" from well to well, that is the wave is translationally invariant and looks the same in every well. The letter "B" means "Back-and-forth" from well to well, that is, the wave flips phase by π but otherwise looks the same in every well. "B" also can mean "Brillouin Band Boundary" since that π-flip is the earmark of the first Brillouin boundary state. (Recall (2.8.18).) However, "A" states also serve as band boundaries, for even numbered gaps. The subscripts "$_1$" and "$_2$" mean C_2 *-symmetric* and *anti-symmetric*, respectively, to reflections through the center of each well, that is, *anti-node* and *node*, respectively. Better subscripts might be the binary "0" and "1" of C_2 ("odd" and "even") but *"1-2"* notation has a long group-theoretical history.

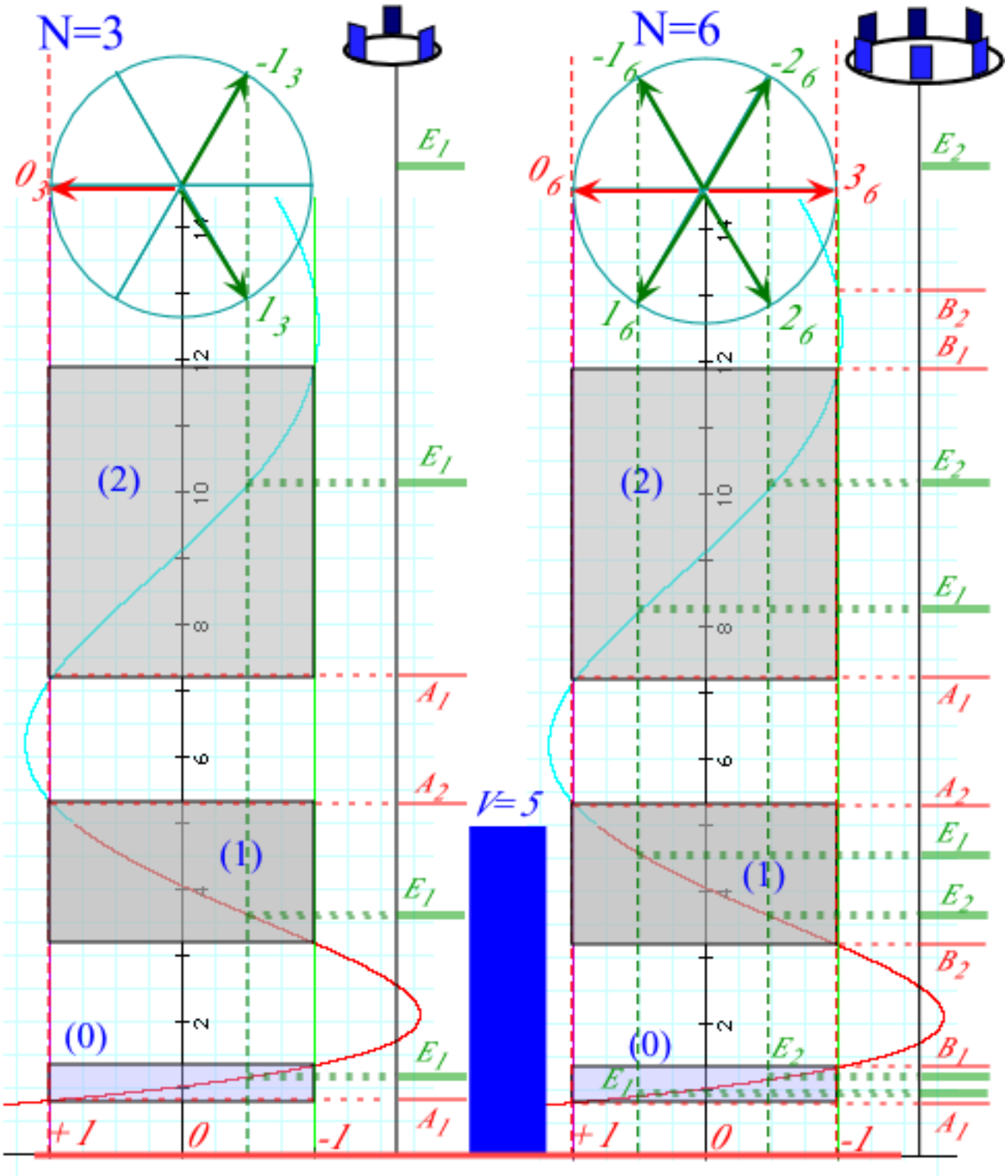

Fig. 14.2.8 Multiplets for V=5.(W=15nm well ,L=5nm barrier) for (N=3)-ring and (N=6)-ring.

The *(N=6)*-ring levels are a repeat-after-12 sequence (A_1, E_1, E_2, B_1)-*(gap)*-(B_2, E_2, E_1, A_2)-*(gap)* while the *(N=3)*-ring levels repeat-after-6 sequence (A_1, E_1,)-*(gap)*-(E_1, A_2)-*(gap)* , a subset of *(N=6)*.

(c) N=6 ring versus N=3, 2, 1 structures

Indeed, the *(N=6)*-well ring energy eigenvalues are exact copies of eigenvalues for *N*-well rings for all the integers *N* that are factors of the integer *N=6*, namely, *N=3*, *N=2*, and *N=1*. Add to this the excellent approximate spectrum of the linear *(N=2)*-well system resonance peaks shown in Fig. 14.2.9, and it appears that *five* different eigenvalue problems are treated in a single stroke!

As we said before, the circular *(N=2)*-well spectrum consists of the KP band boundaries alone, but it has a particular symmetry sequence (A_1, B_1)-*(gap)*-(B_2, A_2)-*(gap)*. Its bands are as empty as its gaps since the (E_1, E_2) pairs of doublets are gone. The circular *(N=2)*-well waves are virtually identical to the to the linear *(N=2)*-well waves shown in Fig. 14.1.11. The difference is due to coupling being cut in half in the linear case. This is reflected in the half-as-big splitting of the (0^+, 0^-)-*(gap)*-(1^+, 1^-)-*(gap)*- etc. sequence in Fig. 14.1.11 and Fig. 14.2.9 which is well approximated by the *(N=6)*-ring levels (E_1, E_2)-*(gap)*-(E_2, E_1)-*(gap)* except that the levels are all singlets as shown in Fig. 14.2.9. ("Sines" only, "cosines" are deleted.) So, finally, the circular *(N=2)*-spectrum (A_1, B_1)-*(gap)*-(B_2, A_2)-*(gap)* is about twice the splitting and encloses linear *(N=2)*-spectrum consisting of inversion doublets (0^+, 0^-)-*(gap)*-(1^+, 1^-)-*(gap)*- etc. in Fig. 14.1.11 and Fig. 14.2.9.

There is an apparent symmetry labeling inconsistency between the three types of doublets.

Circular *(N=2)*-well spectrum: (A_1, B_1)-*(gap)*-(B_2, A_2)-*(gap)* (14.2.14a)

Circular *(N=6)*-well doublets: (E_1, E_2)-*(gap)*-(E_2, E_1)-*(gap)* (14.2.14b)

Linear *(N=2)*-well doublets: (0^+, 0^-)-*(gap)*-(1^+, 1^-)-*(gap)*... (14.2.14c)

The third sequence goes (+,-)-(+,-)-... while the first goes (A,B)-(B,A)-...that is, one "zigs" while the other "zags." How can this be, if the waves are, in fact, virtually the same shape and symmetry?

To answer this, note that the first labels *A* and *B* tell if the wave is even or odd, respectively, to lattice translation or a $2\pi/N$-rotation around the *z*-axis of the *N*-ring. (*N=6* here.) On the other hand, the (+) or (-) labels tell if a wave is odd or even, respectively, to reflection through the barrier between the wells or inversion of the wells. For even *(0), (2), (4),...*bands there is no difference between these two definitions of even and odd, but for odd *(1), (3), (5),...*bands, the two are reversed, hence the "zag" in (14.2.14c).Closer examination of the (E_1, E_2) sine-waves reveals that they, too, are symmetric and anti-symmetric to lattice translation like *A* and *B* , so (14.2.14b) is consistent with the rest of (14.2.14).

(1) Chiral symmetry breaking

Cyclic or circular C_N ring symmetry is called D_N or C_{Nv} symmetry if it also has transverse *180°* rotational symmetry or reflection plane symmetry, in other words, if right and left moving waves have the same speeds. The *A*, *B*, and *E* symmetry labels belong to these higher symmetries. However, they are useless if there is any chiral or *C*-type (Zeeman-like) symmetry breaking that distinguishes right from left. Then the E_m-doublets will be Zeeman or Coriolis-split, and the old $(0)_N$, $(1)_N$, $(2)_N$, .. labels of C_N must be used. The effect of this type of symmetry breaking on C_6 spectra was diagrammed in Fig. 9.3.2 in which the energy hexagon is rotated by an amount determined by the relative left-right coupling phase. That same angle of rotation would apply to the phase hexagon in Fig. 14.2.8. From this one can calculate the Zeeman splitting of an *N*-well KP system.

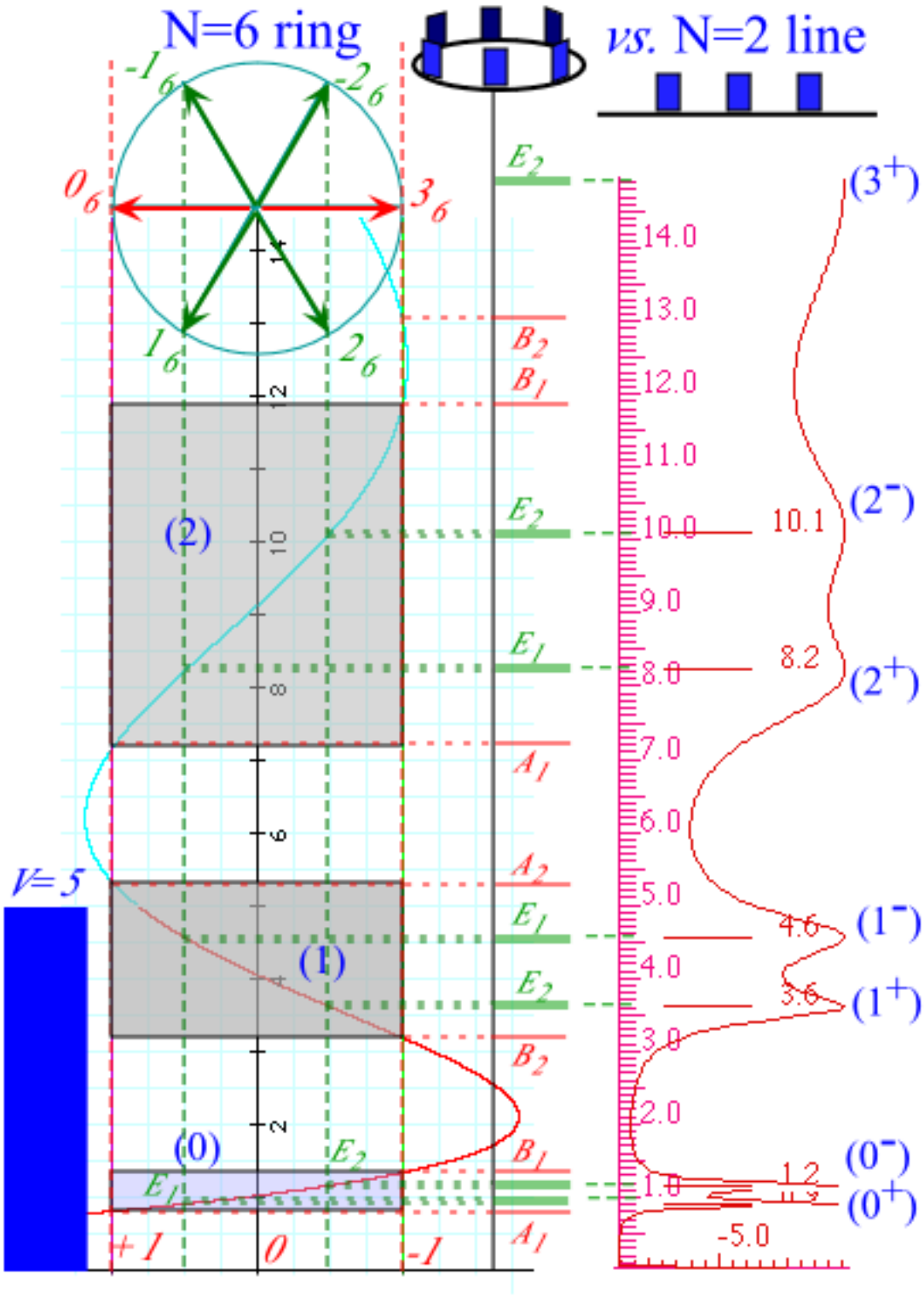

Fig. 14.2.9 Multiplets for (N=6)-ring and (N=2)-line potential. (V=5, W=15nm well ,L=5nm barrier)

(2) Reflection symmetry breaking

In Fig. 14.1.15, we showed that tiny amounts of "dirt" or "micro-symmetry breaking" could totally ruin any multiplet spectral structure and associated perfect 100% transmission properties. On the other hand, it is

possible to obtain quite perfect multiplet structure using "ruined" potentials of the type shown in Fig. 14.2.10 below. It is only necessary that they be identically "ruined" and spaced.

Such a potential, if wrapped onto a ring will also show band multiplet structure quite similar to that which is exhibited in Figs. 14.2.8-9. Furthermore, the moving wave degeneracy would not be lifted unless there was also a chiral or Zeeman-like perturbation as well. This will be discussed further in later chapters.

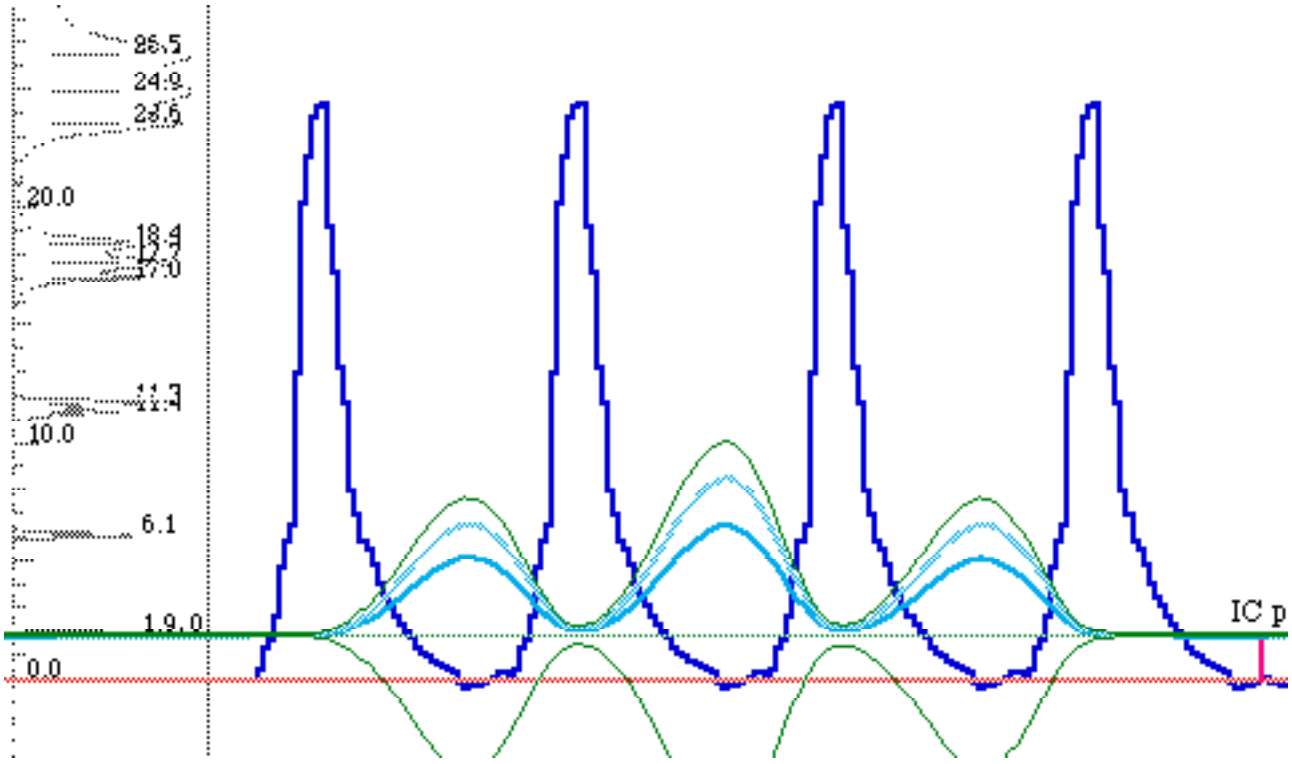

Fig. 14.2.10 Asymmetric wells of (N=4)-line potential still give 100% transmission if repeated perfectly.

(3) Band "smiles": Where BZ waves can still move

The crossing and recrossing of KP band boundaries yields a phenomenon that is peculiar to flat-topped or flat-bottomed potentials such as we have been treating. Parts of what look like "smiles" are seen in the upper left-hand side of Fig. 14.2.7. They are more obvious in a more extensive KP band plot in which the well and barrier have the same value ($L=W=1.0$) while V varies, as shown in Fig. 14.2.11 below.

The crossing points for the "smiles" all fall on energy lines that are perfect squares of even integers in Bohr units. These happen to be the energies for an infinite square well whose width W takes up exactly one quarter of the Bohr ring circumference. The nearly degenerate multiplet bands are seen to be very slowly approaching these asymptotic values.

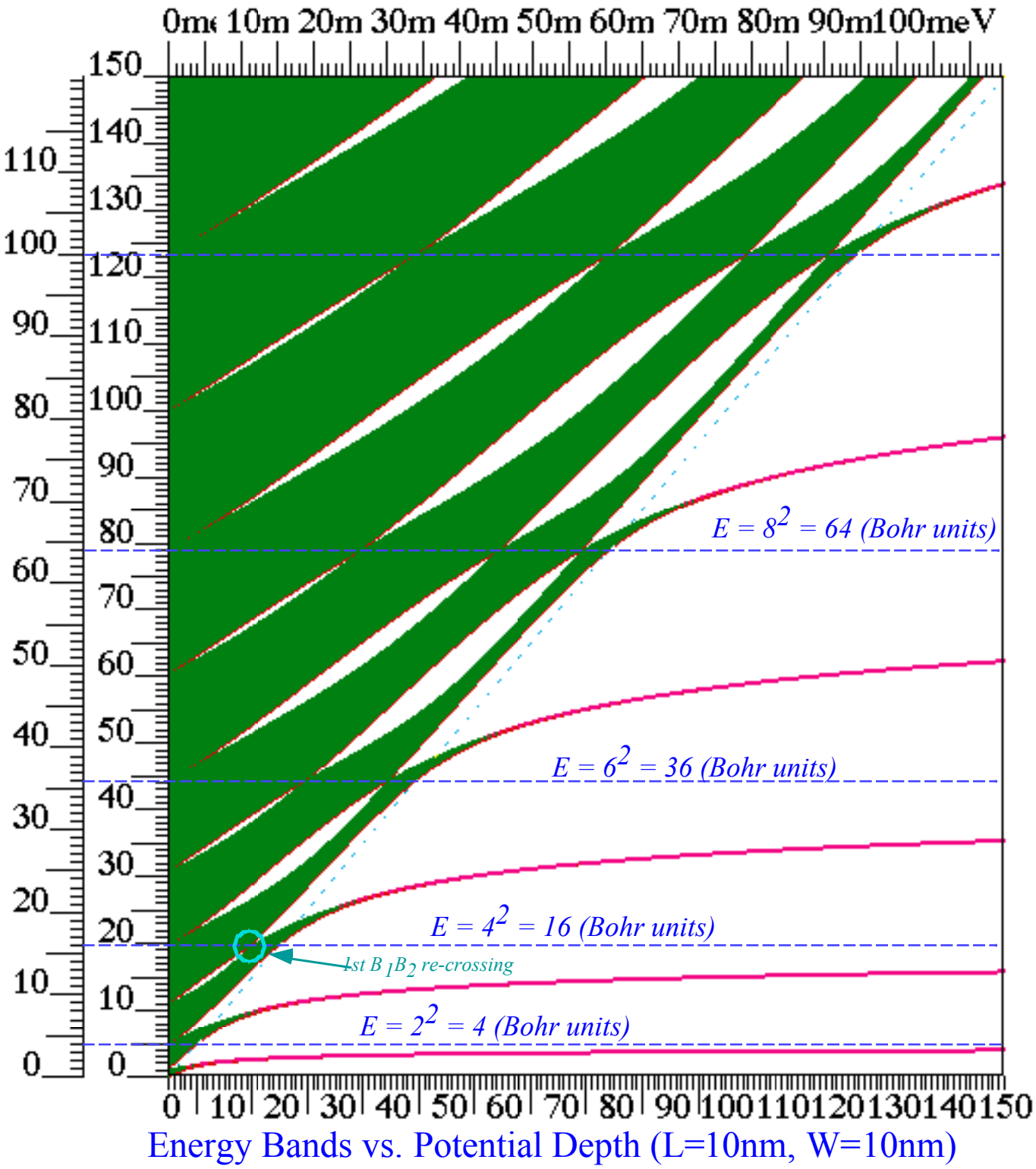

Fig. 14.2.11 Energy E-bands versus barrier height for equal width wells and barriers.

The resonances above the barrier also correspond to these energies but at finite V as shown in Fig. 13.2.6.

The two sides of Fig. 14.2.11 define the energy units for the Bohr problem with no potential ($V=0$) on the left hand side, and the infinite square well ($V=\infty$) to the extreme right hand side. Either extreme displays a quadratic dependence on a quantum number υ which gives the fraction of the maximum wavelength allowed by the boundary conditions for either situation.

For the Bohr limit ($V=0$) the maximal wavelength takes up N lattice spacings of $A = W + L$ or

$$\lambda_0(\upsilon,N)=\frac{N(W+L)}{\upsilon},\quad \text{or:}\quad k_0(\upsilon,N)=\frac{2\pi}{\lambda}=\frac{2\pi}{N(W+L)}\upsilon \qquad (14.2.15a)$$

Here: $\upsilon = 1, 2, 3,..., \infty$. For the box limit ($V=\infty$) the maximal wavelength is twice a well length W or

$$\lambda_\infty(\upsilon)=\frac{2W}{\upsilon},\quad \text{or:}\quad k_\infty(\upsilon)=\frac{2\pi}{\lambda}=\frac{\pi}{W}\upsilon \qquad (14.2.15b)$$

The latter is independent of N and barrier length L since the N wells are no longer speaking to each other. Their waves are totally confined to their respective maximum-security prison wells W. The resulting energy level doublets at $V=0$ and $V=\infty$ are, respectively, the following

$$E_0(\upsilon,N)=\frac{k_0^2}{2}=\frac{2\pi^2}{N^2(W+L)^2}\upsilon^2, \quad (14.2.15c) \qquad E_\infty(\upsilon)=\frac{k_\infty^2}{2}=\frac{\pi^2}{2W^2}\upsilon^2 \quad (14.2.15d)$$

(Natural energy units are used.) For $W = L$, as in Fig. 14.2.11, the values are

$$E_0(\upsilon,N)=\frac{k_0^2}{2}=\frac{\pi^2}{2N^2W^2}\upsilon^2, \qquad (14.2.15e) \qquad E_\infty(\upsilon)=\frac{k_\infty^2}{2}=\frac{\pi^2}{2W^2}\upsilon^2 \quad (14.2.15f)$$

If $N=2$ (two wells on the ring) and $L=1$ (100A=1nm) then E_0 gives the same Bohr unit $(\pi^2/2)/4 = 1.23$ (natural units) as (14.2.11). So, the lowest doublets at $V=0$ and $V=\infty$ are the following with $\upsilon = 1$.

$$E_0(\upsilon,2)=\frac{\pi^2}{8}\upsilon^2, \quad (V=0) \qquad (14.2.15g) \qquad E_\infty(\upsilon)=\frac{\pi^2}{2}\upsilon^2 \quad (V=\infty) \quad (14.2.15h)$$

That is one Bohr-unit (1 $Bu=\pi^2/8$ *nat.u.*) on the left of Fig. 14.2.11 and four Bohr-units on the right.

The infinite-V limit is approached slowly by the energy values. The sine-line solution shows how slowly the asymptotic energies are reached as a function of V and υ. Evanescent waves are gradually squeezed out and the bound state kW approaches multiples of π. (See exercises.) However, we noted that square well resonance kW values occur exactly at multiples of π , since they are not encumbered by evanescence. So, there can be E and V values for which barrier-top wavelengths fit L and inside-the-well wavelengths match W.

$$k_{TOP}=\sqrt{2(E-V)}=\frac{\pi}{L}\upsilon_{TOP}, \quad \text{and} \quad \ell_{WELL}=\sqrt{2E}=\frac{\pi}{W}\upsilon_{WELL}. \qquad (14.2.16)$$

The first non-zero-V solution to the equations (14.2.16) for $W = L$ (in Bohr-units of $Bu=\pi^2/8$) is $E = 16\ Bu$ and $V = 12\ Bu$ located at the corner of the first closed "smile" at $(V,E) = (12,16)\ Bu$ in Fig. 14.2.11. Two wavefunctions corresponding to this "accidentally degenerate" solution are shown in Fig. 14.2.12. Their symmetries are clearly B_1 and B_2 as marked. This is a singular case of exactly degenerate Brillouin zone boundary states. All the $N=2$ eigenstates except these are required to be standing waves. But, the B_1 and B_2 (at the degenerate point only) can make $U(2)$ current carrying eigenstates. It is a case where two eigenchannels resonate simultaneously. It is quite unusual!

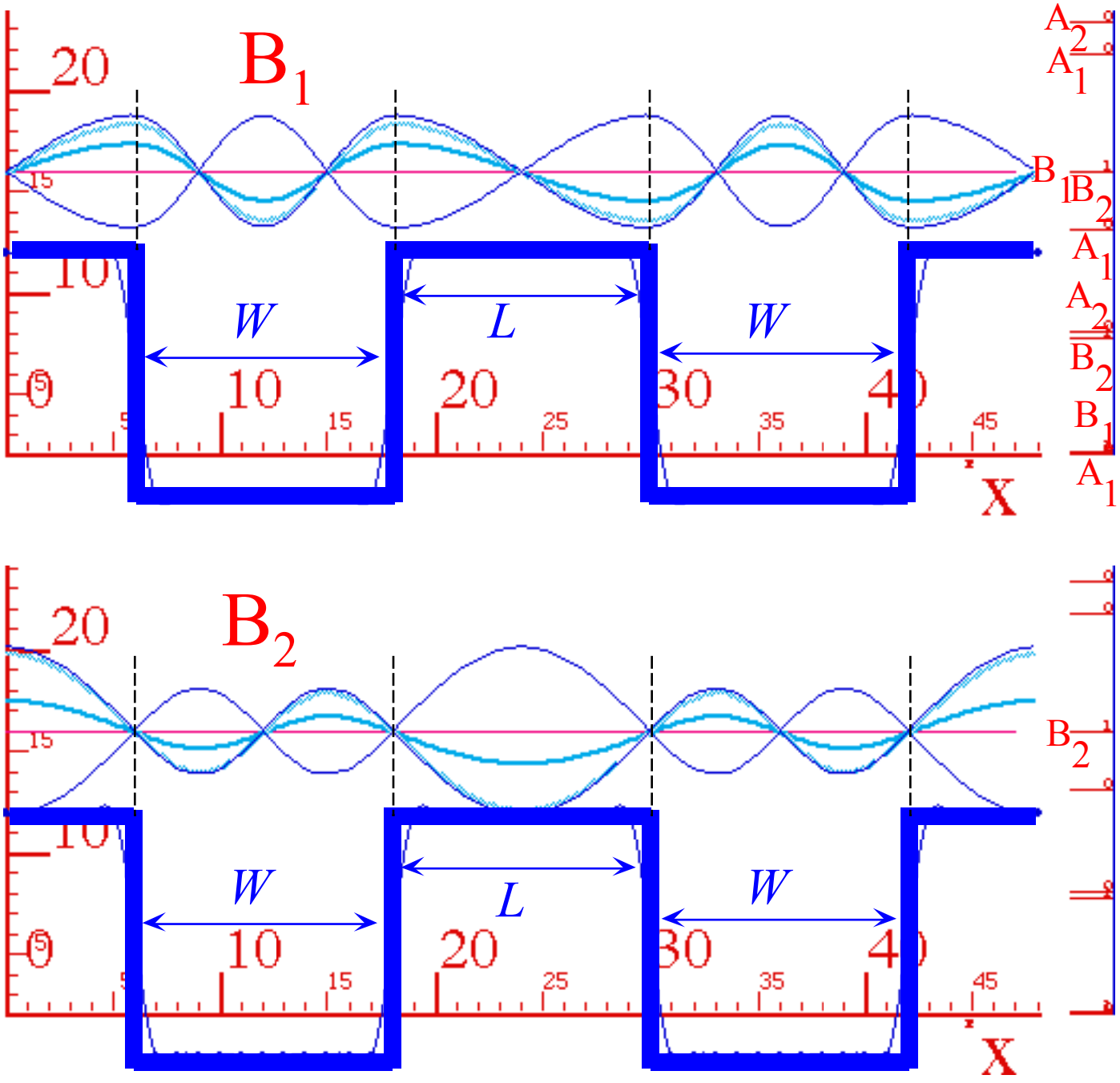

Fig. 14.2.12 Accidentally degenerate (B_1, B_2) doublet at V=12 and E=16.

An expanded view of the *E* vs.*V* plot for *N=2* is shown in Fig. 14.2.13. It shows where the B_1 and B_2 levels cross in order to recover the "normal" (A_1, B_1)-*(gap)*-(B_2, A_2)-*(gap)* symmetry ordering mentioned previously in the discussion of below-barrier levels. Above the barrier, the levels can go wild! (And, they do it with a "smile!") In the higher resonance regions they can get "bent" many times. However, as the barrier value *V* grows they all untwist back to "normal" before descending into the wells. Their prison has strict rules of order!

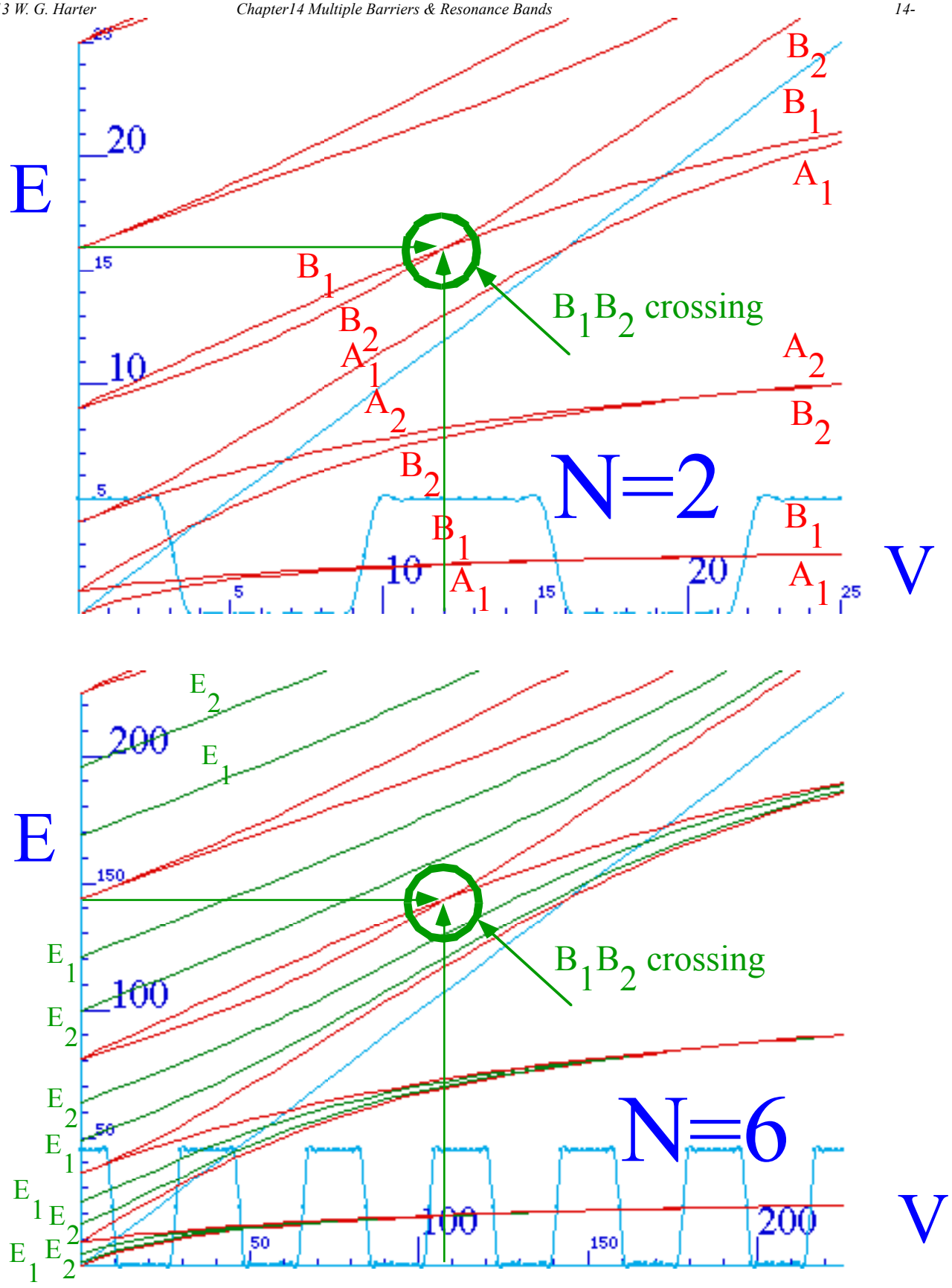

Fig. 14.2.13 (B_1, B_2) crossing for:(N=2) at V=12 and E=16, and (N=6) at V=144 and E=108.

The lower half of Fig. 14.2.13 contains a plot of the same B_1-B_2 level crossing as it appears in the spectrum of a hexagonal $N=6$ Bohr-Bloch lattice of equal square wells. Here, as was done for Fig. 14.2.8, we compare the $N=6$ spectra with that of lesser N which are factors of $N=6$ such as $N = 3, 2,$ and 1.

Note that the B_1-B_2 waves shown for $N=2$ in Fig. 14.2.12 are the same for $N=6$ or any even-N-well ring. The only difference is that the B_1-B_2 waves extend over three times as many lattice-wells since the $N=6$ ring is three times as big as the $N=2$ ring. That is what makes this kind of symmetry analysis powerful; smaller problems are copied into larger ones. Structure of $N=6$ reappears in $N=12, 18, 24$,...

What does change, as we double or triple an N-well, is the number of levels per band, which is always N, and the energy scale or Bohr unit, which according to (14.2.15c) shrinks according to inverse N^2. Both graphs in Fig. 14.2.13 use Bohr energy units exclusively. Each positive energy value that is a perfect square $E_\upsilon = \upsilon^2$ corresponds to a doublet level at the starting point of zero potential $V=0$.

Band splittings occur only for levels for which υ is a multiple of $N/2$, that is, at the beginning of Brillouin zone band boundaries. For $N=6$ these occur for $\upsilon = 3, 6, 9$, ...and so forth, whereas for $N=2$ they occur at every $\upsilon = 1, 2, 3$, ... (except for $\upsilon= 0$) and give rise to a sequence (A_1, B_1)-*(gap)*-(B_2, A_2)-*(gap)*. For $N=2$ there are only two levels in each band and they *are* the band boundaries.

Then as N is tripled from $N=2$ to $N=6$ there must appear three times as many energy levels inside each band. The four new levels appear as moving-wave doublets E_1 and E_2, which lie inside the band boundaries and cannot cross. That the E-doublets remain band-bound is a consequence of the Kronig-Penney (KP) construction shown in Fig. 14.2.8. Moving-wave levels must fall inside the ±1 bounds of the KP functions which define the A-or-B band boundaries. For $N=6$, (A_1, E_1, E_2, B_1)-*(gap)*-(B_2, E_2, E_1, A_2)-*(gap)* is the ususal ordering but A or B pairs may switch places and criss-cross in the "smile" regions.

If N is tripled from $N=2$ to $N=6$ then so are the quantum numbers labeling a particular structure. For $N=2$, the first band splitting happens at $\upsilon=1$. For $N=6$, it happens at $\upsilon=3$. The Bohr-unit energy values for a particular criss-crossing or Bohr level splitting involve squares of integer quantum numbers. So the energy for that level crossing is higher by a factor of three-squared ($3^2=9$). Consequently, all the energy values in the $N=6$ part of Fig. 14.2.13 are nine times the corresponding ones in the $N=2$ version. The B_1-B_2 splitting that happens at $V=12$ and $E=16$ for $N=2$, is scaled up to $V=108$ and $E=144$ for $N=6$.

It is interesting to see what happens for odd-N ring lattices, particularly, $N=1$ and $N=3$. As shown in Fig. 14.2.8, the trigonal $N=3$ spectrum is just the hexagonal $N=6$ structure with "half-a-triangle" consisting of the three levels in the E_2 doublet and B_1 or B_2 singlets removed. (Odd-N spectra cannot have B-type band boundaries. Why?) So the B_1-B_2 crossing and levels leading to it are missing from the $N=3$ or any other odd-N problem. But, there are still plenty of A_1-A_2 crossings!

(6) Bragg reflection...and non-reflection

The exact closing of two band boundaries is unusual and has consequences for current transmission properties. The usual situation of separated band boundaries precludes eigenstates with energy in the gap between bands. However, a non-stationary combination state of, say, a B_1B_2 pair of states, could have any in-between value of energy, and it would beat at a frequency equal to the band-gap energy difference.

The resulting beating is called elementary *Bragg-reflection*. An example is seen in the Fig. 14.2.14 below in which a B_1B_2 combination wave beats or gallops between a left-moving and a right-moving wave while pausing briefly as a standing wave between each gallop. When B_1B_2 levels become degenerate, as in Fig. 14.2.12, the beating stops and each possible wave combination becomes stationary in current and magnitude.

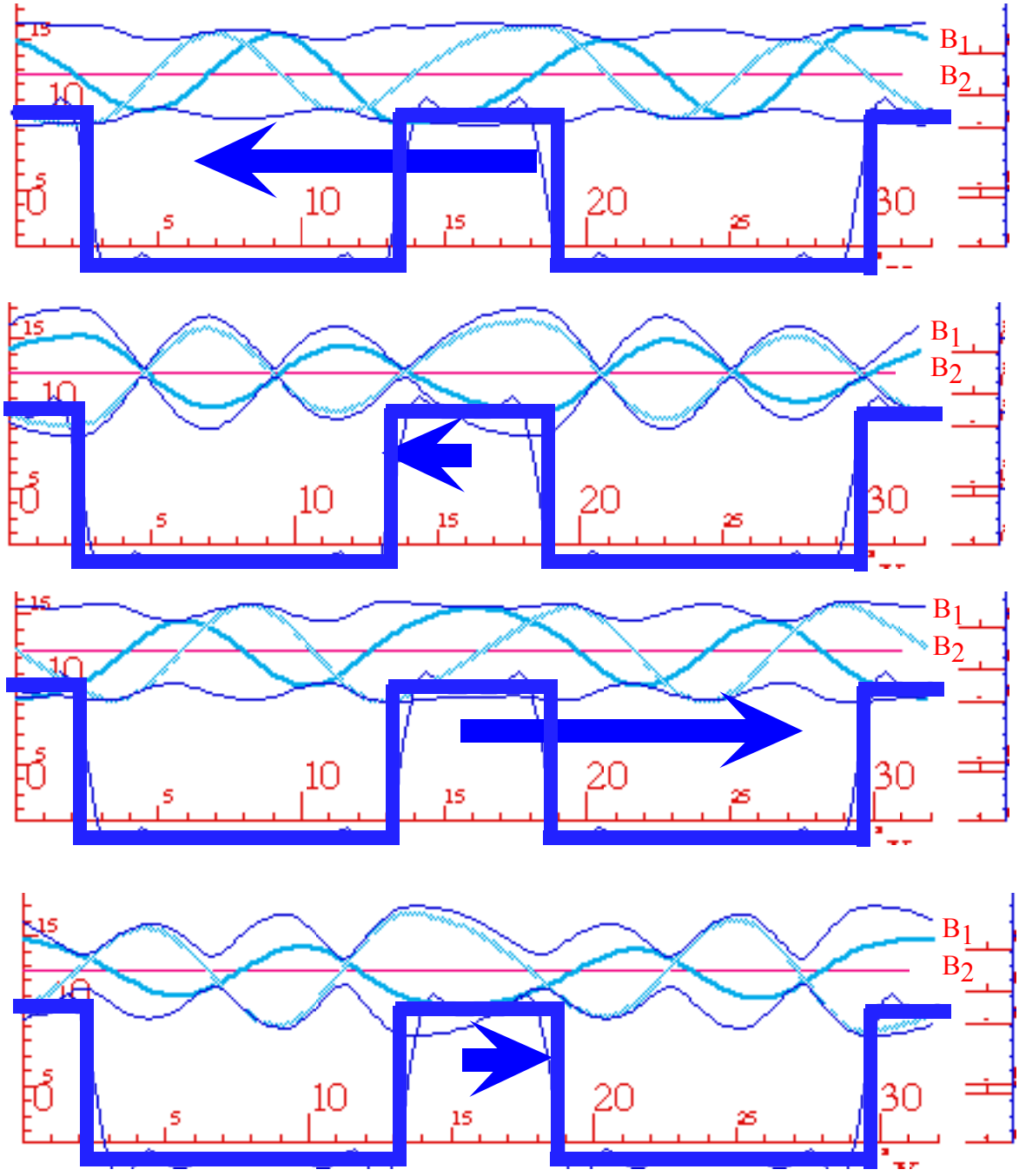

Fig. 14.2.14 Time dependent waves in between a (non-degenerate) B_1B_2 gap. (Elementary Bragg reflection.)

Problems for Chapter 14.

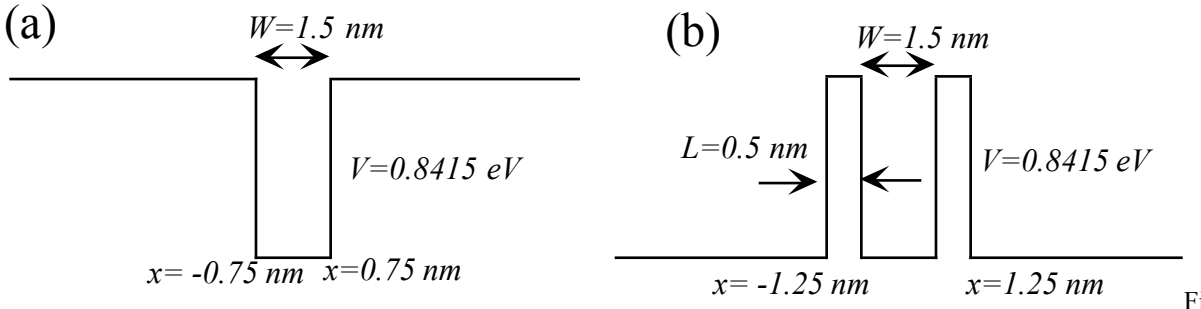

Fig. 1.1

Leapfrogging phases

14.1.1. The eigenchannel phase-shifts for the resonances above the ∞'ly thick walled well (Figure 1.1a above) undergo fairly strong variation for grazing resonances. Pick an energy E = .85eV above the barrier and plot the μ-values as you vary the well bottom V 0.8eV either way. What values of $\mu_{\pm}$ indicate resonance? (Use sine-line solution to tell when resonance occurs.)

Twin Towers vs. Well

14.1.2. Consider two barriers of height V = -0.8415 eV and width L = 0.5nm separated by a width W = 1.5nm. (See Fig. 1.1b)
(a) Find or plot peaks of transmission function belonging to all resonance states below the barriers and first two resonance states above the barriers. Compare with results of Problem 14.1.1. involving the square well in Fig. 1(a).
(b) Calculate and plot both S-matrix eigenchannel waves for the highest two resonances below the barrier tops and the lowest resonance above them.
(c) Compare symmetry and other properties of "resonant" eigenchannel waves vs. "non-resonant" eigenchannel waves with energies in between the resonant transmission peaks.
(c) Pick one resonant case and one non-resonant case and for each combine the eigenchannel states so they make a left-source-channel wave. Plot your results.

Lorentz Fits

14.1.3. Consider the well of depth $V = -1eV$ and width $L = 2.0$ in units of distance of 1.23 nm.
(a) Use the sine-line method to characterize the bound states and first two resonance states.
(b) Derive and plot the transmission and inverse transmission functions for the well with walls reduced from ∞ to a thickness of 0.5.
(d) Discuss how the "bound" state eigenvalues and resonance peaks of this well change when the surrounding walls are reduced from ∞ to a thickness of 0.5. Compare and discuss.
(c) Try fitting Lorentzian functions to the lowest resonance peaks. Are there some good fits? ..bad fits?

Quality:a most important product

14.1.4. In classical resonance theory the *Quality Factor* $Q=\upsilon_0/2\Gamma$ is a key figure of merit as is the related *angular quality* $q=\omega_0/2\Gamma=Q/2\pi$. What do these numbers tell about a resonance?
(First, check and discuss (or correct) the statements after (14.1.8) about resonance amplification being a sum of C_{11} or C_{12} components of barrier matrix (13.3.34a).)
(a) Calculate the number of oscillations or "heart beats" of resonance packet in the time it takes to decay by (14.1.13) by 95% (to 5%) of its amplitude. Relate this to q.
(b) Find the relative probabilty loss ΔP/P per cycle (or per radian) and relate to Q (or q). Give estimates for the E=1.5, 6.1, and 13.4 resonances in Fig. 14.1.6.
(c) Compare results of (b) to Lorentzian theory of Fig. 14.1.9.
Extra credit. (Could be a topic for a paper.)
(d) Does the exact S-matrix for this problem (and others) really have a pole around where we claim it does? (And, does it really matter?)

Delta humps vs. stumps

14.2.1. The effect of a Dirac-delta function potential V(x) = δ(x-a) may be derived directly using the analysis of Sec. 13.3 or as a limit of very narrow and tall "stump" potential.

(a) Derive the C-matrix and S-matrix for a Dirac-delta function potential $V(x) = A\,\delta(x-a)$.
(b) Compare your result to that of a "stump" in the appropriate limit. (Recall Prob. 13.2.1 *Stump*)
(c) Discuss the S-matrix eigenfunctions for $V(x) = \infty\,\delta(x-a)$ and $k=1$, first for $a=0$, and then for general values of a such as $a=\pi/2$. Sketch the wavefunctions.
(d) A line of N equally spaced delta humps should yield band-like or cluster spectra. Derive equations analogous to KP Eq. (14.2.5b) and solve for lowest couple of bands for $N=5$.

Minor Swindle

14.2.2. Consider a line of N identical wells of depth $V = 15$ (in theorist's units with $m/\hbar^2=1$) and length $L = 1.5$ separated by a barrier of width $W=0.5$. Relating the tunneling parameter $S(0)$ between $N=2$ and $N=3$ involved a minor swindle involving a factor of 2 or 1/2. (See right after Eq. (14.1.21).) Discuss this where appropriate.
(a) Use the coupled pendulum model to approximately predict the form of the generic multiplet structure for the cases $N=2$, $N=3$ (in text), $N=4$, and $N=5$ in terms of H and S parameters. Sketch the wavefunctions for each case of the members of the (0) and (1) resonance, that is, the two lowest resonances.
(b) Use the KP equations to obtain a better and more informative approximation to the (0) resonance multiplet band of the four cases in part (a). Compare the splitting of all four.
(c) Use a numerical evaluation or plot of the exact C-matrix calculation such as *BandIt* for the $N=3$ case to obtain exact (0) resonance peaks. Compare to the results of part (b). What additional information does the C-matrix method give over and above the KP method?

Missing Zeros

14.2.3. In Fig. 14.1.21 the lowest $(1)_3$ resonance seems to have 3 nodes in the potential region while the uppermost $(1)_1$ resonance has 5 nodes. However, the middle $(1)_2$ resonance seems to have only 2 nodes and to disobey Schrodinger's theorem that more nodes means more energy.
(a) Is the above counting correct? Discuss and sketch the waves.
(b) Sketch a complete set of S-matrix eigenchannel waves for the (1) resonance triplet.

Open and closed

14.2.4. Consider a familiar square PE with a barrier-well of height $V = 15$ UserUnits, width $W = 1.5$nm and barrier thickness of $L = 0.5nm$. Now, we derive and use its KP function to analyze its band structures and resonances. First, plot its KP function and bands for *0-1eV*.
(a) Locate the resonances of infinite-line super-lattice with 4-wells and 5-barriers.
(b) Locate the eigenvalues of closed-loop super-lattice with 10-wells and 10-barriers.
Use "professional" notation $A_1, A_2, B_1, B_2, E_1, E_2$, etc. where appropriate to label levels.

Sluggish Asymptotes

14.2.5. The quasi-degenerate multiplets in the lower right hand side of Fig. 14.2.11 appear to approach the even square asymptotes rather sluggishly. Prove that they do in fact approach them and give a simple approximate formula for their behavior as a function of barrier height V and well parameters W and L.
(a) Do this first for the case of the Fig. 14.2.11 (W=1=L) and test the formulas.
(b) Do the general formula and test it with Fig. 14.2.7.

Criss-cross

14.2.6. Consider the location of band "smiles" and crossing points shown in Fig. 14.2.11.
(a) Give a formula for the location of crossing points and a table for the ones in Fig. 14.2.11.
(b) Tell which symmetries (A_1, B_1 , B_2, A_2) are involved and track or label their paths to the right side.
(c) Do the general formula and test it with Fig. 14.2.7.
x. (Open ended problem) Suppose that well-to-well phase shift is different for left-moving waves than for right-moving ones and was described by a retardation deficit angle σ introduced in Ch. 2 equation (2.8.15).

Review Topics & Formulas for Unit 5

Kronig-Penney band conditions.

$$\left.\begin{array}{l} (\textit{for } E>V): \quad \cos kW\ \cos \ell L - \dfrac{2E-V}{2\sqrt{E\left(E-V\right)}} \sin kW\ \sin \ell L \\ (\textit{for } E<V): \quad \cos kW \cosh \kappa L + \dfrac{V-2E}{2\sqrt{E\left(V-E\right)}} \sin kW \sinh \kappa L \end{array}\right\} = \cos\phi \qquad (14.2.5b)$$

where rational units are used for energy.

$$\phi = m\frac{2\pi}{N}\ , \qquad k=\sqrt{2E}\ , \qquad \ell=\sqrt{2\left(E-V\right)}\ , \qquad \kappa=\sqrt{2\left(V-E\right)}\ . \qquad (14.2.5c)$$